

1 **Benthic phosphorus cycling in the Peruvian Oxygen**  
2 **Minimum Zone**

3

4 **U. Lomnitz<sup>1</sup>, S. Sommer<sup>1</sup>, A. W. Dale<sup>1</sup>, C. R. Löscher<sup>1</sup>, A. Noffke<sup>2</sup>, K. Wallmann<sup>1</sup>**  
5 **and C. Hensen<sup>1</sup>**

6

7 [1]{GEOMAR Helmholtz Centre for Ocean Research Kiel, Wischhofstr. 1–3, 24148 Kiel,  
8 Germany}

9 [2]{Institut für Seenforschung (ISF) der LUBW, Argenweg 50/1, 88085 Langenargen,  
10 Germany}

11 Correspondence to: U. Lomnitz ([ulomnitz@geomar.de](mailto:ulomnitz@geomar.de))

12

## 13 **Abstract**

14 Oxygen minimum zones (OMZs) that impinge on continental margins favor the release of  
15 phosphorus (P) from the sediments to the water column, enhancing primary productivity and  
16 the maintenance or expansion of low-oxygen waters. A comprehensive field program in the  
17 Peruvian OMZ was undertaken to identify the sources of benthic P at six stations, including  
18 the analysis of particles from the water column, surface sediments and pore fluids as well as  
19 in situ benthic flux measurements. A major fraction of solid phase P was bound as particulate  
20 inorganic P (PIP) both in the water column and in sediments. Sedimentary PIP increased with  
21 depth in the sediment at the expense of particulate organic P (POP). The ratio of particulate  
22 organic carbon (POC) to POP exceeded the Redfield ratio both in the water column ( $202 \pm$   
23  $29$ ) and in surface sediments ( $303 \pm 77$ ). However, the POC to total particulate P (TPP = POP  
24 + PIP) ratio was close to Redfield in the water column ( $103 \pm 9$ ) and in sediment samples  
25 ( $102 \pm 15$ ). This suggests that the relative burial efficiencies of POC and TPP are similar  
26 under low oxygen conditions and that the sediments underlying the anoxic waters on the Peru  
27 margin are not depleted in P compared to Redfield. Benthic fluxes of dissolved P were  
28 extremely high (up to  $1.04 \pm 0.31 \text{ mmol m}^{-2} \text{ d}^{-1}$ ), however, showing that a lack of oxygen  
29 promotes the intensified release of dissolved P from sediments, whilst preserving the  
30 POC/TPP burial ratio. Benthic dissolved P fluxes were always higher than the TPP rain rate to  
31 the seabed, which is proposed to be caused by transient P release by bacterial mats that had  
32 stored P during previous periods when bottom waters were less reducing. At one station  
33 located at the lower rim of the OMZ, dissolved P was taken up by the sediments indicating  
34 ongoing phosphorite formation. This is further supported by decreasing porewater phosphate  
35 concentrations with sediment depth, whereas solid phase P concentrations were comparatively  
36 high. At this site, the POC/TPP and POC/PIP ratios dropped from average water column  
37 values (close to Redfield for POC/TPP and POC/PIP  $\sim 250$ ) to very low sedimentary ratios of  
38  $\sim 7$  (POC/TPP and POC/PIP), indicative of intensive P enrichment in the sediments.

## 39 **1 Introduction**

40 Phosphorus is an essential nutrient; it serves as an energy carrier for all living species and is a  
41 limiting macronutrient for marine primary production on geological time scales [Ingall and  
42 Jahnke, 1994; Föllmi, 1996; McManus et al., 1997; Filippelli, 2002; Paytan and McLaughlin,  
43 2007; Tsandev et al., 2012; Ruttenberg, 2014]. Due to its impact on marine primary

44 production, the oceanic phosphorus inventory modulates the atmospheric CO<sub>2</sub> level and  
45 Earth's climate [Ganeshram et al., 2002; Wallmann, 2003; Ingall, 2010]. Hence, it is crucial  
46 to understand feedback mechanisms of the P cycle to make future predictions.

47 Particulate and dissolved phosphorus in the ocean originate from terrestrial chemical  
48 weathering of the P containing mineral group of apatite [Filippelli, 2002]. Only around 30%  
49 of the P discharged to the oceans is potentially bioavailable [Compton et al., 2000] as  
50 dissolved P, inorganic P adsorbed to minerals or associated with metal oxides and P bound  
51 within particulate organic matter. However, the largest fraction of the fluvial P is trapped in  
52 estuaries or buried in continental margin sediments and thereby removed from the P cycle  
53 before it reaches the open ocean [Compton et al., 2000]. The delivery of P to the sediments in  
54 the open ocean is mainly composed of organic and inorganic P associated with the export of  
55 organic detritus and other particles from the photic zone. P adsorbed to minerals such as Mn  
56 and Fe (oxyhydr)oxides [Föllmi, 1996; Delany, 1998; Faul et al., 2005] are further sources, as  
57 well as P input from fish debris that is may be particularly important in productive upwelling  
58 regions [Suess, 1981; Schenau and DeLange, 2001; Diaz-Ochoa et al., 2009; Noffke, 2014].

59 P cycling is strongly affected by redox-dependent processes. P can be scavenged by Fe  
60 (oxyhydr)oxides in oxic sediment and released across the sediment-water interface due to the  
61 reduction dissolution of Fe (oxyhydr)oxides in anoxic sediments [Sundby et al., 1986; Slomp  
62 et al., 1998]. Furthermore, recent studies showed that sulfur bacteria found in surface  
63 sediments of anoxic environments can internally store and release P under oscillating redox  
64 conditions [Ingall and Jahnke, 1997 and references therein]. Therefore, these organisms are a  
65 key player for the modulation of porewater P concentrations and benthic P release to the  
66 water column.

67 Additionally, hypoxic or anoxic conditions favor the precipitation of P in the form of  
68 authigenic carbonate fluorapatite (CFA) [Froelich et al., 1988; Suess and von Huene, 1988;  
69 Goldhammer et al., 2010; Ingall, 2010; Schenau and De Lange, 2000]. For non-upwelling  
70 areas, the required phosphate oversaturation in the porewaters has been attributed to the  
71 reductive dissolution of P bearing Fe (oxyhydr)oxides [e.g. Ruttenger et al, 1993, Slomp et  
72 al., 1996]. In contrast, the CFA formation in sediments of the Namibian upwelling area was  
73 linked to microbial P release into the porewaters [Schulz and Schulz, 2005].

74 The resulting feedback on oceanic primary production and atmospheric O<sub>2</sub> and CO<sub>2</sub> levels  
75 triggered by changes in benthic P sequestration is still unclear. Presently, three opposing

76 views have been raised: (1) Intensified phosphate release from the sediments to the water  
77 column caused by an expansion of low oxygen waters [Ingall and Jahnke, 1994; Stramma et  
78 al., 2008] could stimulate the primary production in the surface waters [Wallmann, 2003].  
79 This, in turn, may lead to a more intensified oxygen demand and a positive feedback with  
80 benthic P release [Slomp and Van Cappellen, 2007; Wallmann, 2010; Moffit et al., 2015]. (2)  
81 A negative feedback on P release has been postulated based on observations of CFA mineral  
82 precipitation in the present-day oxygen depleted upwelling areas [Schulz and Schulz, 2005;  
83 Arning et al., 2009a; Arning et al., 2009b; Goldhammer et al., 2010; Cosmidis et al., 2013].  
84 Being a major sink for bioavailable P [Delaney, 1998; Ingall, 2010], it has been argued that  
85 the expansion of OMZs may increase the CFA precipitation in the sediments and thus  
86 mitigate benthic phosphate release [Ganeshram et al., 2002; Goldhammer et al., 2010; Ingall,  
87 2010]. (3) A third scenario suggests that the formation of CFA is in balance with enhanced P  
88 release from anoxic sediments, implying that the dissolved oceanic P inventory is largely  
89 unaffected by oxygen concentrations [Delaney, 1988; Anderson et al., 2001; Roth et al.,  
90 2014]. These conflicting scenarios show that there is further need to explore the benthic-  
91 pelagic P cycling in oxygen deficient environments in order to enable improved predictions.

92 In this study, we explore P cycling in the Peruvian OMZ to identify and quantify P sources to  
93 the sediment and the return of inorganic dissolved P back to the water column. Our data set  
94 comprises samples of particulate matter from the water column as well as porewater, sediment  
95 and samples of filamentous sulfur bacteria. We present in situ benthic phosphate fluxes,  
96 particulate matter C/P ratios for water column particles and surface sediments, P burial fluxes  
97 and relative abundances of sulfur bacteria for 6 stations along the depth transect across the  
98 Peruvian shelf at 12°S. From a mass balance for P cycling in the sediments, we conclude that  
99 the benthic P sources and sinks were, in general, imbalanced during our sampling campaign.

100

## 101 **2 Study Area**

102 The study area is located in the center of the Peruvian OMZ at 12°S covering the shallow  
103 shelf from ~70 m water depth to mid-slope depths of about at ~400 m (Fig. 1). During our  
104 sampling campaign in January 2013 neutral or slightly negative El Niño-Southern Oscillation  
105 (ENSO) conditions dominated (<http://www.cpc.ncep.noaa.gov>) and the bottom water oxygen  
106 concentrations were below detection limit of the Winkler titration ( $5 \mu\text{mol L}^{-2}$ ) down to ~ 450

107 m water depth (Fig. 1, Table 1). Below the OMZ, oxygen concentrations increased to 19 and  
108 53 $\mu$ M at 770 m and 1025 m water depth, respectively. Nitrate concentrations were below 12  
109  $\mu$ M from 128 to 407 m water depth (Table 1). During the measuring period, the bottom water  
110 at station I (74 m) was sulfidic and depleted in nitrate (Table 1; Sommer et al., in review).

111 The oxygen deficient waters off Peru belong to one of the world's most prominent OMZ.  
112 Southeasterly trade winds that are driven by the Pacific Subtropical Anticyclone engender  
113 offshore transport of surface waters and upwelling of subsurface waters from the poleward  
114 propagating Peru undercurrent (PUC) [Strub et al., 1998]. These water masses are oxygen  
115 depleted and rich in nutrients, favoring primary production of up to 3.6 g C m<sup>-2</sup> d<sup>-1</sup> in surface  
116 waters [Pennington et al., 2006]. As a consequence, the intense oxygen consumption induced  
117 by the degradation of sinking particulate organic matter and a sluggish ventilation induce the  
118 development of a strong OMZ. Based on the definition that the oxycline of an OMZ is at ~22  
119  $\mu$ M [Fuenzalida et al., 2009], the Peruvian OMZ extends from approximately 50 – 700 m  
120 water depth. The greatest upwelling strength is reached during austral winter and spring  
121 between 5 and 15°S [Strub et al., 1998]. The phases of strong upwelling are followed by high  
122 rates of primary production in austral summer. The coastal area off Peru displays a highly  
123 variable hydrographic regime. Especially during positive ENSO periods coastal trapped  
124 waves emerging from equatorial Kelvin waves in the equatorial East Pacific occur frequently  
125 [Gutiérrez et al., 2009 and references therein; Mosch et al., 2012]. Consequently, the  
126 thermocline and the oxycline shift downwards by ca. 100 m and bottom water oxygen  
127 concentrations can increase from practically zero to around 100  $\mu$ M in days to weeks  
128 [Gutiérrez et al., 2008; Schunck et al., 2013; Graco et al., 2016]. Seasonally, bottom waters of  
129 the shelf (75 m) can transition from oxic or hypoxic between austral winter/spring (low  
130 primary production) to anoxic throughout the rest of the year [Noffke et al., 2012].  
131 Furthermore, porewater uranium (U) profiles at 11°S indicate variable redox conditions at the  
132 upper rim of the OMZ possibly related to ENSO [Scholz et al., 2011]. The shelf area above  
133 200m water depth is therefore characterized by non-steady state conditions, whereas the  
134 oxygen concentrations in the core OMZ (~200-400 m water depth) are predominantly below  
135 detection limit throughout the year.

136 The sediments of the Peruvian OMZ have POC contents ranging from 15-20 wt. % within the  
137 OMZ and > 5 wt. % below the OMZ and on the shelf [Dale et al., 2015]. The fine-grained,  
138 diatomaceous mud lens between 11°S and 15°S accumulates under low PUC bottom water

139 velocities in 50 to 500 m water depth [Krissek et al., 1980]. This favors high sedimentation  
140 rates, carbon preservation and burial [Suess et al., 1987; Dale et al., 2015]. Further down, at  
141 mid-slope depth, a high energy regime favoring erosive settings leads to the formation of  
142 phosphorites [Reimers and Suess, 1983; Glenn and Arthur, 1988; Arning et al., 2009b; Mosch  
143 et al., 2012]. Another interesting observation between 70 and ~ 300 m of water depth is the  
144 occurrence of mat-forming filamentous sulfur bacteria [Mosch et al., 2012]. Bacterial mats  
145 not conspicuous below 300 to 400 m water depth, and instead foraminiferal sands are more  
146 common.

147

### 148 **3 Methods**

149 Sampling of water column particulate matter and sediment cores as well as the deployment of  
150 the benthic landers BIGO I and II (Biogeochemical Observatories) was conducted along the  
151 12°S depth transect during the RV *Meteor* cruise M92 in January 2013. The geographical  
152 position and water column properties for the main stations are reported in Table 1. The data  
153 set on in situ phosphate fluxes comprised 10 stations from 74 to 989 m water depth. The water  
154 column particle sampling was performed at 6 stations from 74 to 407 m water depth. These  
155 stations are considered as main stations and for consistency the stations are numbered  
156 according to the data set published in Dale et al. (2015). Hydrographic parameters and oxygen  
157 concentrations were obtained by deploying a CTD/rosette equipped with a Seabird oxygen  
158 sensor (detection limit is 5  $\mu$ M) calibrated by Winkler titration.

#### 159 **3.1 Water column particles**

160 Particulate matter was filtered using water from Niskin bottles from the CTD/rosette and  
161 analyzed for total particulate phosphorus (TPP), particulate inorganic phosphorus (PIP) and  
162 particulate organic carbon (POC) concentrations. Following Labry et al. (2013), we expect the  
163 PIP phase to be comprised of inorganic P phases originating from abiotic particulate P as well  
164 as inorganic P from biogenic particulate P. Abiotic PIP comprises detrital P associated to  
165 minerals from terrigenous sources. Biotic PIP is composed of orthophosphates,  
166 pyrophosphates and polyphosphates within eukaryotic and prokaryotic cells.

167 Between three and six water depths were sampled per station. The water was filled into 10 L  
168 PE containers rinsed beforehand with ultrapure water (MilliQ). The containers were shaken  
169 before filtration which was performed within 24 h after sample retrieval. Approximately 2 to  
170 4 L of seawater were filtered through pre-weighed and combusted (450°C, 5h) 0.7 µM  
171 Whatman GF/F filter using a seawater vacuum pump and Duran bottle top filters. After  
172 filtration, all filters were immediately frozen at -20°C. At the shore-based laboratory the GF/F  
173 filters were dried over night at 45°C, and divided into 3 equally sized pieces using a scalpel.  
174 The total filtered water volume was divided by three to calculate elemental concentrations on  
175 each filter section assuming homogenous coverage of particles on the filters.

### 176 **3.1.1 Total particulate phosphorus (TPP), particulate inorganic phosphorus** 177 **(PIP) and particulate organic phosphorus (POP)**

178 The determination of TPP and PIP concentrations by combustion and colorimetric methods  
179 has been described by Asahi et al. (2014), Aspila et al. (1976), Loh and Bauer (2000) and  
180 others. However, the combustion and acid dissolution (HTC/hydrolysis) that has been applied  
181 for PIP-determination is limited by the fact that polyphosphates are only partly hydrolysed,  
182 but provides the best compromise compared to other methods (Labry et al., 2013). Although  
183 polyphosphates are underestimated, it includes intracellular P that is often dominant in  
184 plankton and only small amounts of organic P. In the case of TPP we used the Aspila (1976)  
185 method without an oxidant (e.g. MgSO<sub>4</sub>) during combustion, which underestimates the TPP  
186 concentration in water column particles. However, for the sediments, the results following the  
187 Aspila (1976) method were compared to total digestions, showing an average recovery of the  
188 Aspila method of approximately 102%. In two samples we found an overestimation in total  
189 digestion of more than 100% and in one sample an underestimation of 32%, possibly due to  
190 heterogeneity of the samples caused by very small phosphorite granules.

191 Filter segments for TPP concentration were combusted at 550°C for 90 min and afterwards  
192 soaked with 20 ml 1 N hydrochloric acid (HCl) and shaken for 24 h at room temperature.  
193 Then, the solution was filtered and 0.35 ml triple reagent (40 ml 9.8 N sulfuric acid, 12 ml  
194 ammonium molybdate and 4 ml potassium antimonyl tartrate solution) and 0.175 ml ascorbic  
195 acid and 3 ml 1 N HCl were added to 3.75 ml of the sample solution. Then, 0.3 ml of 12.5 N  
196 sodium hydroxide (NaOH) was added to the solution before colorimetric measurement of  
197 phosphate at 880 nm using a Hitachi U-2001 photospectrometer. This was done because test

198 runs with the standard series revealed that the slope of the calibration curve was not steep  
199 enough to measure the low phosphate concentrations expected. To resolve this issue, the pH  
200 of the solution was slightly increased using NaOH. Measurements were accompanied using a  
201 standard series consisting of 8 standards ranging from 5 to 100  $\mu\text{M PO}_4^{3-}$ , prepared from a  
202 Merck phosphate stock solution. We used 0.75 ml of each standard for the standard series and  
203 treated each of them in the same manner as described above. The samples were measured  
204 undiluted due to low concentrations and the technical detection limit of a 1 cm cuvette.  
205 Hence, we used 3.75 ml of the filtered sample solution, added the reagents mentioned above  
206 and divided the concentrations by a factor of 5 to adjust the results to those of the standard  
207 series. A factor of 0.02 was used to transform the concentration unit to  $\mu\text{mol L}^{-1}$ . The amount  
208 of filtered water (f) refers to 1/3 of the total filtered water volume (f is different for each  
209 sample):

$$\text{TPP or PIP } [\mu\text{mol L}^{-1}] = \frac{[\text{PO}_4^{3-}] \cdot 0.02}{5 \cdot f}$$

210 The same procedure was performed for PIP without the combustion step. The POP  
211 concentration was calculated by the difference of the measured (as phosphate) TPP and PIP  
212 concentrations.

### 213 **3.1.2 Organic carbon concentration**

214 The filter sections for the analysis of POC concentration were fumed with 37 % HCl  
215 overnight to remove inorganic carbon, dried and wrapped into tin caps. Samples were  
216 measured by flash combustion with a Carlo Erba elemental analyzer (NA1500). The  
217 analytical precision and detection limit were 0.04 dry wt. %. The water column POC  
218 concentrations are given in  $\mu\text{mol L}^{-1}$ .

### 219 **3.2 Porewater and solid phase analysis**

220 Sediment cores were recovered using video-guided multiple corers (MUC) equipped with  
221 PVC liners with an inner diameter of 10 cm. The porewater and solid phase sub-sampling was  
222 performed immediately after recovery in an argon-filled glove bag at in situ seafloor  
223 temperature. The bottom water was siphoned with a plastic tube and filtered through cellulose  
224 acetate filters. Afterwards, the cores were sectioned into 0.5 cm intervals from 0-5 cm



225 sediment depth and 1 cm intervals afterwards. The sediment samples were filled into  
226 centrifuge tubes and the porewater was separated from the sediments by centrifuging for 20  
227 min at 4500 rpm. The supernatant porewater was filtered through cellulose acetate filters  
228 inside the glove bag. Samples were immediately analyzed for total dissolved phosphate  
229 ( $\text{TPO}_4$ ) and dissolved ferrous iron ( $\text{Fe}^{2+}$ ) after porewater extraction using a Hitachi U-2001  
230 spectrophotometer. The analyses were performed according to the standard techniques  
231 described in Grasshoff et al. (1999). A sediment subsample was taken from each sediment  
232 depth and stored refrigerated in pre-weighed air-tight plastic cups to determine the water  
233 content, porosity and total organic carbon (TOC) content. The residual sediments were stored  
234 frozen at  $-20^\circ\text{C}$  (sediment and filter samples) and the porewater samples were refrigerated at  
235  $4^\circ\text{C}$  for land-based analytics.

236 The TOC concentration (in  $\mu\text{mol mg}^{-1}$ ) of freeze-dried and ground sediment samples was  
237 determined by flash combustion in a Carlo Erba Elemental Analyzer (NA 1500). For POC  
238 determination, samples were decalcified with 2.5 N HCl prior to the measurement. Solid  
239 phase TPP and PIP concentrations were measured according to the method of Aspila et al.  
240 (1976) in a similar manner as described before for the water column particles. 50 mg of  
241 freeze-dried and ground sediment were digested in 1N HCl for a minimum of 24 hours to  
242 dissolve the sedimentary PIP phase. Sediment portions analyzed for TPP were combusted at  
243  $550^\circ\text{C}$  for 90 min before adding 1 N HCl. The solutions were filtered and the reagents  
244 mentioned above were added prior to measurement. We used the sedimentary reference  
245 standards SDO-1 (Devonian Ohio Shale, USGS; Govindaraju, 1994) and MESS-3 (Marine  
246 Sediment Reference Material, Canadian Research Council) and replicate measurements of  
247 samples to ensure measurement accuracy. The standard series applied to the measurements  
248 covered a concentration range from 5 to 100  $\mu\text{M}$ .

249 To determine the terrigenous P input to the sediments, and to calculate the TPP burial flux  
250 (for calculation see section 3.6 and Table 2), sediments were analyzed using total digestion.  
251 About 100 mg of freeze dried and ground sediment was digested in hydrofluoric acid (40%,  
252 supra pure), nitric acid (65%, supra pure) and perchloric acid (60%, supra pure). For  
253 measurement accuracy the reference standards SDO-1 and MESS-3 as well as methodological  
254 blanks were included in the analysis. The aluminum concentration in the digestion solutions  
255 was measured using an inductively coupled plasma optical emission spectrometer (ICP-OES,  
256 Varian 720 ES). The relative standard deviation (RSD) for [Al] was found to be  $< 1\%$ .

257 The XRD data of core 107MUC23 from 407 m water depth were obtained from  
258 approximately 1 g of freeze dried and ground sediment in the lab of the University of Bremen.

### 259 **3.3 POC in relation to various fractions of P (POC/xP ratios)**

260 The molar POC/xP ratios (where xP = TPP, PIP or POP) of the water column particles at  
261 stations I, IV and V were calculated from measurements on two filter samples per water  
262 depth. For these samples a minimum and maximum value was calculated. For the other  
263 stations III, VI and VIII, only one filter sample per water depth was available. Here, we  
264 assumed an average natural variability calculated from the duplicate measurements of stations  
265 I, IV and V for each P species (supplementary material). For sediment samples we calculated  
266 a standard deviation from repeated measurements of the sediment standards MESS-3 and  
267 SDO-1 (supplementary material).

### 268 **3.4 Benthic lander fluxes**

269 Benthic lander deployments were performed at 10 stations along the 12°S transect (I to X  
270 according to Dale et al., 2015). In situ benthic fluxes were obtained using the two BIGOs I  
271 and II (BIGO: Biogeochemical Observatory). They were equipped with two circular flux  
272 chambers (internal diameter 28.8 cm, area 651.4 cm<sup>2</sup>) [Sommer et al., 2009]. An online video-  
273 controlled launch system allowed precise placement of the BIGO at the seafloor directly  
274 located beneath the particle sampling stations in the water column and in proximity to the  
275 multi-corer stations. After a 4 hour rest period at the seafloor during which surrounding  
276 bottom water was periodically flushed into the chamber, the chambers were slowly driven  
277 into the sediment. The BIGOs stayed for 28 hours at the seafloor, while 8 water samples per  
278 chamber were taken via glass syringes. In order to obtain bottom water background  
279 information, additional samples were taken every 8 hours from the ambient bottom water.  
280 Phosphate concentrations in the syringe samples were measured on board using an auto  
281 analyzer. The standard series covered a concentration range from 0.05 to 3.5 μM. The fluxes  
282 were calculated from the slope of linear regression of all 8 data points versus the sampling  
283 time (supplementary material) and corrected for the water volume in the chamber and the  
284 dead volume of the 1 m long Vygon tubes connecting the syringes with the flux chambers.  
285 The error caused by the dilution from the dead volume of these tubes was calculated from the  
286 chloride concentration measured in the syringe samples. Benthic lander TPO<sub>4</sub> fluxes for most

287 sites are based on two replicate chamber measurements. The uncertainty given for the TPO<sub>4</sub>  
288 fluxes is the difference between the minimum and maximum fluxes from the average of the  
289 two benthic chambers. At two stations (IV and V), it was only possible to calculate the flux  
290 from one chamber. For further details on the benthic flux measurements during the M92  
291 cruise see Dale et al. (2015).

### 292 **3.5 Diffusive flux calculations**

293 The diffusive fluxes of TPO<sub>4</sub> and Fe<sup>2+</sup> from the sediment to the bottom water were calculated  
294 by applying Fick's First Law of diffusion:

$$295 \quad F_{TPO_4/Fe^{2+}} = -\phi D_{SED} (d[C]/dx) \quad (1)$$

296 where the term  $d[C]/dx$  describes the concentration gradient between the bottom water and the  
297 first porewater sample of the surface sediment divided by the corresponding sediment depth  
298 (0.25 cm or 0.5 cm) and  $\phi$  is the porosity of the surface sediment. The diffusion coefficient,  
299  $D_{SED}$ , for sediments was calculated according:

$$300 \quad D_{SED} = D_{SW}/\theta^2 \quad (2)$$

301 The diffusion coefficients for TPO<sub>4</sub> and Fe<sup>2+</sup> ( $D_{SW}$ ) under standard conditions (298.15 K and 1  
302 bar) were taken from Li and Gregory (1974) and corrected for the in situ temperature and  
303 pressure using the Stokes-Einstein equation. The tortuosity ( $\theta^2$ ) was derived from the  
304 sediments porosity according to Boudreau (1996):

$$305 \quad \theta^2 = 1 - \ln(\phi^2) \quad (3)$$

306 Uncertainty in the diffusive flux was calculated at St. I as the difference between the fluxes  
307 calculated from two separate sediment cores. For the other stations, only one core was  
308 available to calculate the flux.

### 309 **3.6 Mass balance of benthic phosphorus cycling**

310 To investigate benthic P cycling quantitatively, a mass balance was developed considering P  
311 input, P burial, and P release. The equations for the P mass balance calculations are shown in  
312 Table 2. Under steady state conditions, the total P rain rate should balance the P buried in the  
313 sediments and the benthic TPO<sub>4</sub> flux (Eq. 4 in Table 2). The rain rates of particulate P

314 delivered to the sediments are differentiated in inorganic P ( $RR_{PIP}$ ) (Eq. 5 in Table 2) and  
315 organic P ( $RR_{POP}$ ) (Eq. 6 in Table 2). The rates were calculated using the POC/xP ratio of the  
316 water column particles that were taken as close as possible to the seafloor at each station (2-5  
317 m above ground) and the POC rain rate ( $RR_{POC}$ ) (Table 4 and supplementary material).  $RR_{POC}$   
318 for the same stations along the 12°S transect were previously calculated by Dale et al. (2015)  
319 as the sum of the measured benthic DIC flux and the POC accumulation rate. The terrigenous  
320 P input ( $RR_{Pterr}$ ) (Eq. 7 in Table 2) can be estimated by multiplying the solid phase Al  
321 concentration of the first sediment sample by the mass accumulation rate (MAR) [Dale et al.,  
322 2015] and a P/Al ratio of 0.02 that characterizes the P/Al ratio of riverine particles originating  
323 from the continent [Viers et al., 2009].

324 The P burial flux ( $F_{Pbur}$ ) (Eq. 8 in Table 2) was calculated by multiplying the mass  
325 accumulation rate (MAR) and the average solid phase P concentration of the first 11 sediment  
326 centimeters ( $P_{11}$ ) (11 cm is due to our sampling resolution). This approach was chosen  
327 according to Dale et al. (2015) who also calculated POC accumulation rate for the OMZ  
328 stations (i.e. not on the shelf or below the OMZ) using the elemental average concentration of  
329 the first 10 cm of sediment. MAR (Eq. 9 in Table 2) was calculated from the sedimentation  
330 accumulation rate ( $\omega_{acc}$  in  $cm\ y^{-1}$ ), dry bulk density ( $\rho_{dry}$ ; in  $g\ cm^{-3}$ ) and the average porosity  
331 of the sediments at the lower core end ( $\phi_{\infty}$ ). Sedimentation accumulation rates were  
332 determined from particle-bound  $^{210}Pb_{xs}$  measurements using a modeling approach. A detailed  
333 method description and the values used for this work are published in Dale et al. (2015). The  
334 error derived from modeling the sedimentation rate was given as 20 % and propagates to all  
335 subsequent calculations where it was used.

### 336 **3.7 Freeze/thaw experiments**

337 In order to determine the amount of polyphosphate stored in sulfide-oxidizing bacteria,  
338 foraminifera and other bacteria we conducted additional sediment experiments at all transect  
339 stations, except station IV. Sediments from MUC corers were sliced into 1 cm thick slices  
340 from the surface sediment to 10 cm sediment depth. Before phosphate analysis, sediment  
341 slices were repeatedly frozen at -80°C and defrosted in order to burst microbial cells and  
342 release the internally stored P to the porewater.

### 343 **3.8 Molecular quantification of filamentous bacteria**

344 In order to quantify the abundance of filamentous microbes at the benthic boundary layer, we  
345 used a molecular approach. Nucleic acid purification was performed on 0.5 g sediment  
346 following established protocols [Bertics et al., 2013]. DNA was quality checked on an agarose  
347 gel and quantified using a Nanodrop spectrophotometer (Peqlab, Erlangen, Germany). 16S  
348 rDNA fragments were taken from a previously generated metagenome from this region  
349 (GenBank Bioproject PRJNA280940) and the respective sequence counting's were deposited  
350 at GenBank (ID KU312264-KU312267). Sequencing was carried out in the Institute of  
351 Clinical Molecular Biology at Kiel University. Sequences were analyzed using a Clustal W  
352 alignment tool on Mega 6 [Tamura et al., 2013]. A qPCR primer and probe set was  
353 established using the Primer Express software (Life Technologies, Carlsbad, USA) with the  
354 forward primer 5' AGAAGCACCGGCTAACTCTG-3' , the reverse primer, 5' -  
355 CCAGGTAAGGTTCTTCGCGT-3' and the probe 829-Thioploca 5'-  
356 GGATTAATTTCCCCAACAT-3' [Teske et al., 1995]. Primers and probes were tested *in*  
357 *silico* on the Silva database and cross amplification was excluded on a variety of 16S rDNA  
358 clones. The qPCRs were performed in technical duplicates on a ViiA7 system (Life  
359 Technologies, Carlsbad, USA) as previously described [Löscher et al., 2014] using 1x  
360 TaqMan PCR buffer (Life Technologies, Carlsbad, USA), 2.5 pmol  $\mu\text{L}^{-1}$  TaqMan probe, 5  
361 pmol  $\mu\text{l}^{-1}$  of each primer, 400 ng  $\mu\text{l}^{-1}$  bovine serum albumin (to avoid PCR inhibition without  
362 affecting standard curves or detection limits), 3  $\mu\text{l}$  PCR water, and 5  $\mu\text{l}$  of either standard  
363 DNA or environmental sample. A plasmid containing the target sequence was used to  
364 generate a standard dilution series for absolute quantification. The melting temperature was  
365 set to 50°C. A theoretical detection limit of 4 copies per PCR reaction was calculated. The  
366 results of the analysis are given in copies  $\text{g}^{-1}$  of 16S rDNA sequences of sulfur bacteria that  
367 are related to Marithioploca.

368

## 369 4 Results

### 370 4.1 P composition of water column particulate matter and surface sediments

#### 371 4.1.1 TPP, PIP, POP and POC concentrations

372 The TPP concentrations ranged from 0.02 to 0.2  $\mu\text{mol L}^{-1}$  in the water column particles and  
373 from 0.04 to 2.37  $\mu\text{mol mg}^{-1}$  in the surface sediments (supplementary material). Overall, the  
374 profiles along the transect show no significant trends through the water column (Fig. 2A). The  
375 highest concentrations occurred in the surface waters around 10 m of water depth. At stations  
376 I, V and VIII (74, 195 and 407 m) the TPP concentrations slightly increased close to the  
377 seafloor, whereas at the other stations no such trend was observed (Fig. 2A and  
378 supplementary material). In the sediments the TPP concentrations slightly decreased with  
379 sediment depth, except at station VIII (407 m). Here, the highest sedimentary TPP  
380 concentrations across the transect were found at 2.25 cm sediment depth (17  $\mu\text{mol mg}^{-1}$ ).  
381 Below that depth the concentrations decreased, but remained high compared to the other  
382 stations.

383 The PIP and POP concentrations (water column and sediments) generally followed the trends  
384 of the TPP profiles and contributed roughly equally to TPP. The PIP fraction accounted for 21  
385 to 74 % of TPP in the water column particles (Fig. 3), similar as reported in previous studies  
386 [Paytan et al., 2003; Faul et al., 2005; Benitez-Nelson et al., 2007; Lyons et al., 2011; Sekula-  
387 Wood et al., 2012]. At stations I, VI and VIII (74, 244 and 407 m), the PIP concentrations  
388 were larger than POP. The opposite occurred at station V (195 m) where the POP fraction was  
389 clearly larger than the PIP fraction throughout the entire water column. In comparison to the  
390 water column particles, the PIP fraction was larger than POP in most samples reaching  
391 between 48 to 98% of TPP. However, the strongest deviation between PIP and POP  
392 concentrations was found in the sediments of station VIII (407 m) where the PIP  
393 concentration was up to a factor of  $\sim 50$  larger than the POP concentration and comprised up  
394 to 98% of TPP. XRD data from that station revealed that 7 to 16 wt.% of the sediments  
395 consisted of apatite and other particulate P (data not shown).

396 The particulate organic carbon concentrations ranged from 2.2 to 17.6  $\mu\text{mol L}^{-1}$  in the water  
397 column particles and from 2.8 to 13.4  $\mu\text{mol mg}^{-1}$  in the surface sediments. Within the water  
398 column the highest concentrations occurred in the surface water samples, while the

399 concentration measured at station VI (244 m) is about 5 times higher than compared to other  
400 samples from the same water depth. Below the surface water concentration peak, the  
401 concentrations were on average  $7 \mu\text{mol L}^{-1}$  with distinct depth trends. The sedimentary POC  
402 concentrations were on average  $7.7 \mu\text{mol mg}^{-1}$  for the whole transect. Overall, the POC  
403 concentrations showed little variability with sediment depth. At station III, VI and VIII (128,  
404 244 and 407 m) the concentrations increased slightly with sediment depth. At station I (74 m)  
405 the concentration decreased slightly with sediment depth.

## 406 **4.2 Particulate organic carbon to phosphorus (POP, PIP, TPP) ratios**

### 407 *POC/POP ratios*

408 The molar POC/POP ratios of the water column particles and of the surface sediments were  
409 consistently higher than the Redfield ratio at all stations (Fig. 2B). The average POC/POP  
410 ratio of the water column particles was  $202 \pm 29$ . There was no clear trend through the water  
411 column, except slightly increasing ratios between the deepest water column samples and the  
412 surface sediment samples. In the surface sediments, the ratios increased within the upper 6 cm  
413 with an average POC/POP ratio of  $303 \pm 77$ . Station VIII (407 m) is an exception and here the  
414 ratio decreased to 81 within the first  $\sim 2$  cm of sediment and then strongly increased to  $\geq 600$ .

### 415 *POC/PIP ratios*

416 The average POC/PIP ratio of the water column particles was  $248 \pm 34$ . Similar to the  
417 POC/POP ratios, there was no significant trend through the water column. At the majority of  
418 the stations, the ratios decreased close to the seabed. The average POC/PIP ratio of the  
419 surface sediments was  $184 \pm 34$  and almost invariable with water depth. In the sediments, the  
420 ratios showed no significant down-core trend. At station VIII (407 m) the ratio in the  
421 sediment showed a dramatic decreased compared to the water column, with an average of 7,  
422 similar to the POC/TPP ratios (below).

### 423 *POC/TPP ratios*

424 The POC/TPP ratios of the water column particles and surface sediments consistently varied  
425 around the Redfield ratio. The exceptions are station I (74 m) and the deepest station (Sta.  
426 VIII, 407 m). At station I, the sediments showed significantly lower than Redfield ratios with  
427 an average of 69 in the surface sediments. The average POC/TPP ratio of the surface

428 sediments at station VIII (407 m) was 7. Between the deepest water column sample and the  
429 first sediment sample, the POC/TPP ratios were rather constant without a consistent trend,  
430 again with the exception of station VIII (407 m) where the ratios decreased sharply.

### 431 **4.3 In situ benthic chamber fluxes**

432 The benthic lander  $\text{TPO}_4$  fluxes ( $F_{\text{TPO}_4}$ ) are presented in Table 3 and Fig. 4A. Positive fluxes  
433 are defined as directed from the sediments into the water column. The highest  $\text{TPO}_4$  flux  
434 along the depth transect of  $1.04 \pm 0.31 \text{ mmol m}^{-2} \text{ d}^{-1}$  occurred at station I (74 m). Below 74 m  
435 water depth, fluxes decreased by at least a factor of 3 to  $0.2 - 0.3 \text{ mmol m}^{-2} \text{ d}^{-1}$  at 144 m water  
436 depth. Measurements at station V (198 m) showed a slightly increased  $\text{TPO}_4$  flux of  $0.44 \pm$   
437  $0.07 \text{ mmol m}^{-2} \text{ d}^{-1}$ , while the fluxes measured at 244 m (St. VI) and 306 m (St. VII) decreased  
438 to the before mentioned levels. At 407 m water depth (St. VIII) the  $\text{TPO}_4$  flux was negative,  
439 indicating a phosphate uptake by the sediment. Below the OMZ, the fluxes increased to  
440 slightly positive values, but remained low at  $0.06$  and  $0.02 \pm 0.02 \text{ mmol m}^{-2} \text{ d}^{-1}$ .

#### 441 **4.3.1 Comparison of benthic chamber $\text{TPO}_4$ fluxes and diffusive $\text{TPO}_4$ fluxes**

442 The measured benthic chamber  $\text{TPO}_4$  fluxes and the calculated diffusive  $\text{TPO}_4$  fluxes showed  
443 large discrepancies. The calculated diffusive fluxes were consistently higher than the benthic  
444 fluxes (Table 4, Fig. 4B). In contrast to the in situ measured benthic chamber  $\text{TPO}_4$  release  
445 rates, the calculation of diffusive  $\text{TPO}_4$  fluxes relies on bottom water and porewater  $\text{PO}_4^{3-}$   
446 concentrations. A subsurface  $\text{PO}_4^{3-}$  peak occurred at all stations in the uppermost depth  
447 interval at 0-0.25 cm causing a large concentration gradient between the bottom water and the  
448 porewater  $\text{PO}_4^{3-}$  concentrations (Fig. 7). Even though the measured benthic  $\text{TPO}_4$  fluxes  
449 exceeded the fluxes that could be generated by TPP degradation by a factor of approximately  
450 6, the diffusive  $\text{TPO}_4$  fluxes were still higher (Table 4). Hence, the diffusive  $\text{TPO}_4$  flux will  
451 be referred to as potential  $\text{TPO}_4$  flux in the following.

### 452 **4.4 TPP burial fluxes and TPP burial efficiency**

453 The P burial fluxes decreased with increasing water depth (Table 4). Station I (74 m) showed  
454 by far the highest P burial flux with  $0.23 \text{ mmol m}^{-2} \text{ d}^{-1}$ . In contrast the P burial efficiency at  
455 this station (Eq. 10) was comparatively low reaching only 26 %. At Station VIII (407 m), the



456 TPP burial flux was  $0.03 \text{ mmol m}^{-2} \text{ d}^{-1}$  and the P burial efficiency exceeded 100 % due to the  
457 uptake of dissolved P from ambient bottom waters.

#### 458 **4.5 Molecular analysis and relative abundance of filamentous sulfur bacteria**

459 Molecular analysis indicated the presence of *Marithioploca*-related bacteria in the surface  
460 sediments (0-5 cm) [Salman et al., 2011]. Our analysis may, however, underestimate the  
461 absolute abundance of these organisms due to a self-splicing mechanism of the 16S rDNA  
462 gene (Salman et al., 2012) and is therefore only indicative of their relative abundance.

463 The relative abundance of *Marithioploca*-related bacteria decreased with increasing water  
464 depth (Table 4). Highest relative abundance with more than 4000 copies  $\text{g}^{-1}$  sediment was  
465 found at station I (74 m), decreasing by more than a factor of 20 to 190 copies  $\text{g}^{-1}$  sediment at  
466 station VIII (407 m).

467

### 468 **5 Discussion**

#### 469 **5.1 POC/xP ratios in water column particles and sediments**

470 In order to characterize the fate of P in oxygen deficient waters and sediments we determined  
471 POC/xP ratios from both environments. Previous studies focused either on the water column  
472 or on the sediments [Anderson et al., 2001 and references therein; Benitez-Nelson et al., 2004;  
473 Faul et al., 2005; Jilbert et al., 2011; Lyons et al., 2011; Sekula-Wood et al., 2012]. The  
474 present data set provides a more complete insight into compositional changes and allows us to  
475 more rigorously constrain the sedimentary P mass balance compared to earlier studies [Ingall  
476 and Jahnke, 1994; Mort et al., 2010; Kraal et al., 2012; Noffke, 2014].

477 Both water column particles and the surface sediments from the Peruvian OMZ displayed  
478 POC/POP ratios above Redfield, indicating depletion of organic P relative to organic C.  
479 Similar observations have been reported before from this and other regions of the ocean [Loh  
480 and Bauer, 2000; Benitez-Nelson et al., 2004; Faul et al., 2005; Franz et al., 2012 and others].  
481 Preferential remineralization of P phases from sinking particles should lead to increasing  
482 POC/POP ratios with increasing water depth, as observed in oxygenated areas of the ocean  
483 [reviewed by Ruttenberg, 2014]. However, in the anoxic Cariaco Basin, no such preferential P

484 mineralization was noted [Benitez-Nelson et al., 2004]. Our results also showed no clear  
485 decrease in the POC/POP ratio in the water column, with the possible exception of St. I and  
486 VIII. Higher than Redfield POC/POP ratios were observed at Peru on a previous occasion,  
487 and may instead be driven by the C-to-P composition of the diatomaceous phytoplankton  
488 communities [Franz et al., 2012] rather than preferential P dissolution or other controls such  
489 as the input of terrestrial plant material with high POC/POP ratios.

490 Preferential POP over POC remineralization in anoxic sediments remains controversial [Ingall  
491 and Van Cappellen, 1990; Ingall and Jahnke, 1994; Colman et al., 1997; Anderson et al, 2001;  
492 McManus et al, 1997; Ruttenberg, 2003; Jilbert et al, 2011]. Our results, however, also  
493 showed no clear trend across all stations. At station I, IV and VI (74, 141 and 244m) the  
494 POC/POP increased with sediment depth indicating preferential POP over POC  
495 remineralization. At station III (128 m) this trend occurred only in the upper cm and at station  
496 V (195 m) no preferential POP over POC remineralization was found. POC/POP ratios at  
497 station VIII (407 m) showed a POP enrichment over the upper 2 cm of the sediment. Below  
498 this depth, there was a sudden increase in POC/POP ratios, which is likely due to intense POP  
499 remineralization and subsequent authigenic formation of phosphorites (sink-switching, see  
500 section 5.2.3).

501 Another interesting finding pointing to sink-switching can be found in the POC/POP and  
502 POC/PIP ratios of the deepest water column particle sample and the first sediment sample at  
503 stations I, IV, VI and VIII (74, 141 and 407 m). Increasing POC/POP and decreasing  
504 POC/PIP ratios indicate that POP is converted into PIP while the TPP content of the sediment  
505 is conserved (Fig. 2A and B). In agreement with similar findings in anoxic sediments  
506 [Ruttenberg and Berner, 1993; Faul et al., 2005 and others] we assume that the observed POP  
507 to PIP transformation is due to the formation of CFAs. However, our results emphasize that  
508 sink-switching is obviously occurring at the interface between bottom waters and sediments.

509 Interestingly, the water column POC/TPP ratios were close to Redfield ratio. This could be an  
510 effect of surface adsorption of P on phytoplankton as previously described by Sanudo-  
511 Wilhelmy et al. (2004). Those authors investigated different species of *Trichodesmium* from  
512 the Atlantic Ocean and found that the intracellular P pool was strongly depleted relative to C,  
513 whereas the combination of the intracellular plus the surface adsorbed P was close to the  
514 Redfield ratio. Although we did not exactly differentiate between internal and external P

515 pools, and considering that additional P sources like terrigenous P are less important (see  
516 section 5.2.1), our results generally support the findings of Sanudo-Wilhelmy et al. (2004).  
517 However, future studies are required to substantiate this hypothesis.

518 Sedimentary POC/TPP ratios were also close to Redfield, except at station I and VIII (74 and  
519 407 m). Thus, on the one hand, the sink switching mechanism operates efficiently under low  
520 oxygen conditions and on the other hand, the relative degradation of TPP and POC are not  
521 changing from the water column to the sediments (Fig. 2B). This is an important finding  
522 because at first sight this observation seems to be inconsistent with the long-standing  
523 paradigm that low oxygen conditions promote the enhanced release of dissolved P from  
524 sediments [Van Cappellen and Ingall, 1996]. However, it should be noted that marine  
525 sediments covered by oxygenated bottom waters display molar POC/TPP ratios ranging from  
526 about 10 to 50 [Baturin 2007]. These ratios are much lower than Redfield because P is  
527 retained in sediments via adsorption, authigenic mineral precipitation such as Fe  
528 (oxyhydr)oxides and microbial P sequestration [Ingall and Jahnke, 1994], and because POC is  
529 more efficiently degraded under aerobic conditions [Hedges et al., 1999, Wallmann, 2010]. In  
530 contrast, our data set implies that oxygen deficiency causes a shift of POC/TPP ratios to  
531 values closer to Redfield compared to oxygenated regions, which is due to both, the enhanced  
532 preservation of POC (Dale et al., 2015) and release of dissolved phosphate under low oxygen  
533 conditions. It remains puzzling why the extreme P depletion observed in some black shale  
534 sequences (e.g. POC/TPP > 3000, Ingall and Jahnke, 1994) are not found in modern anoxic  
535 sediments such as those on the Peru margin.

## 536 **5.2 P mass balance**

537 P release rates from sediments underlying oxygen deficient waters are strongly enhanced  
538 compared to oxygenated marine settings, especially in the Peruvian OMZ [Noffke et al., 2012  
539 and 2016]. Nonetheless, the sources for the enhanced P release are still not completely  
540 identified. The widely held view is that POP raining from the water column to the sediments  
541 represents the main source for sedimentary P in high productive areas like the Peru upwelling  
542 system [Delaney, 1998; Filippelli, 2008]. Mass balance approaches that resolve the P  
543 regeneration versus burial in oxygen deficient environments by combining sedimentary data  
544 and benthic P fluxes are rare [Ingall and Jahnke, 1994; Ingall et al., 2005; Mort et al., 2010;  
545 Kraal et al., 2012; Noffke, 2014]. These studies are all based on sediment data only, that is,

546 the external P input to the sediments is estimated or ignored. Furthermore, the study areas  
547 were often not covered by fully anoxic bottom waters. Noffke (2014) presented an approach  
548 that combines measurements of solid phase P speciation, sediment burial fluxes and benthic  
549 chamber flux measurements for a mass balance on benthic P cycling in the Peruvian OMZ.  
550 Interestingly, the measurements on the solid phase P speciation revealed that organic P  
551 accounted for only 18-37% of the total sedimentary P on the shelf and upper slope [Noffke,  
552 2014]. Furthermore, it was found that P bound to Fe (oxyhydr)oxides and terrigenous P was  
553 of minor importance for the total sedimentary P inventory. However, authigenic Ca-P with a  
554 high amount of fish-P accounted for up to 47% of the total P in sediments down to 300 m  
555 water depth and for up to 70% in sediments below 300 m water depth. Consequently, Noffke  
556 (2014) suggested that authigenic Ca-P phases are an additional major P source besides  
557 organic P for benthic P release in the Peruvian OMZ.

558 Their mass balance approach was solely based on benthic work and has large uncertainties  
559 regarding the particulate P input from the water column. Our approach includes the particulate  
560 organic and inorganic P input from the water column, benthic P flux measurements and the P  
561 burial fluxes and is based on the steady state assumption that the P input has to be sufficient to  
562 maintain the benthic P flux and P burial flux. The P mass balance calculations (Table 4)  
563 illustrate the variability in TPO<sub>4</sub> release and burial as well as in the magnitude of particulate  
564 organic (Fig. 5A) and particulate inorganic P input (Fig. 5B) across the transect. Following  
565 the general assumption that POP is the major P phase delivered to the sediments [Delaney,  
566 1998; Filippelli, 2008], we first calculated whether the rain rate of POP (RR<sub>POP</sub>) to the  
567 seafloor can account for the measured benthic P fluxes (F<sub>TPO<sub>4</sub></sub>) and P burial fluxes (F<sub>P<sub>bur</sub></sub>) (Fig.  
568 5A, Table 4). However, as already suggested by Noffke et al. (2012 and 2014), the POP  
569 fraction is far too small to balance the measured benthic fluxes in the Peruvian OMZ. The  
570 POP rain rates calculated along the transect can account for only 25 to 48% of the measured  
571 TPO<sub>4</sub> fluxes (Fig. 5A), suggesting likely the presence of an additional inorganic source of  
572 dissolved phosphate [Noffke, 2014]. Similar to previous studies [Paytan et al., 2003; Faul et  
573 al., 2005; Benitez-Nelson et al., 2007; Lyons et al., 2011; Sekula-Wood et al., 2012], we  
574 found that the PIP fraction in water column particles ranging from 75 to 407 m water depth  
575 comprises between 21-74% of TPP (Fig. 3). In the sediments, the average PIP fraction rises to  
576 48-98% of TPP (Fig. 3). Furthermore, POC and PIP were correlated ( $r^2=0.74$ ) in the water  
577 column particles indicating highly reactive material.

578 The mass balance approach including the PIP rain rate to the seafloor (Fig. 5B) allows the  
579 depth transect to be divided into two sections. The transect section I (station I, 74 m and III,  
580 128 m) is characterized by high P input and release rates. The calculations on the P budget  
581 show a balance between the particulate P input, the benthic P fluxes and the P burial fluxes  
582 within the error margin ( $\pm 20\%$ ). In transect section II (stations IV, 141 m, V, 195 m and VI,  
583 244 m), the P input decreases drastically (Fig. 5B, Table 4) whereas the benthic P fluxes are  
584 still comparatively high. The distinct mismatch in P input and P output prevails as the  
585 particulate P rain rates supported only 37 to 53 % of the measured TPO<sub>4</sub> fluxes and calculated  
586 burial fluxes. This leads to the question: What drives the excess TPO<sub>4</sub> release in the core of  
587 the Peruvian OMZ?

### 588 **5.2.1 Additional P input**

589 Besides the particulate matter raining to the sediments, other potential other P sources can be  
590 considered. Firstly, riverine transported material from the continent may be an additional  
591 source of P to the sediments. Due to fast sinking speed and laterally dominated transport it is  
592 possible that this P fraction is at least underrepresented on the filter samples. In order to  
593 provide a maximum estimate for the contribution of the terrigenous P input to the sediments,  
594 this fraction was calculated using the mass accumulation rate of Al in the first centimeter of  
595 sediment and an average molar P/Al-ratio (Table 2) of 0.02 for riverine suspended particles  
596 [Viers et al., 2009]. The resulting terrigenous P flux accounted for 5-19 % of the total P input,  
597 which is insufficient to explain the observed discrepancies in the P budget of transect section  
598 II (Table 4, Fig. 4C, 5B).

599 Laterally transported particles enriched in P from the very shallow shelf could be an  
600 additional P source [e.g. Jahnke, 1990]. However, the particles would need to be strongly  
601 enriched in P, which is not the case. In addition, this would have to be reflected in the  
602 POC/TPP ratios of the surface sediments in transect section II (Fig. 2B). The ratios are not, or  
603 only slightly, enriched in TPP compared to the water column particles, which leads to the  
604 conclusion that lateral transport of P-enriched particles to the sediments is an unlikely  
605 candidate for the missing P source.

606 Another alternative is the existence of an additional PIP phase supplied by fast sinking  
607 material (e.g. P containing fish scales; Suess, 1981) that was not sampled during CTD casts  
608 and hence underrepresented on our filter samples. Díaz-Ochoa et al. (2009) showed that fish P

609 can make up to 20% of the total sedimentary P inventory in the shelf sediments of the  
610 Peruvian OMZ. Fish P input should be depicted in low sedimentary POC/TPP ratios  
611 compared to the water column particles. Since this difference is not observed it is likely that  
612 fish debris can be ruled out for closing the P budget during the sampling campaign.  
613 Theoretically, sediments need to be composed of particles having POC/TPP ratios between  $11$   
614  $\pm 1$  and  $25 \pm 12$  (Table 4) to maintain the measured P release rates in transect section II. It  
615 seems unlikely that the mismatch in the P mass balance is caused by additional particles  
616 deposited at the seabed since their POC/TPP ratio would need to be much lower than any  
617 value observed in our data set.

## 618 **5.2.2 Non steady state scenarios – internal sedimentary P pools**

619 Besides an additional P input to the sediments from the water column, episodic dissolution of  
620 particulate P within the sediment could contribute to the excess P release [Noffke et al.,  
621 2012]. This could include P solubilized from Fe (oxyhydr)oxides or the degradation of  
622 internally stored polyphosphates within sulfide-oxidizing bacteria. Driving factors could  
623 include the temporal variability in bottom water oxygen and nutrient concentrations induced  
624 by the passage of internal Kelvin waves and/or interannual variability related to El Niño and  
625 La Niña [Gutiérrez et al., 2008].

626 It is well recognized that the sedimentary cycles of Fe and P are strongly linked [e.g. Sundby  
627 et al., 1986]. Fe (oxyhydr)oxides are expected to be important carriers for phosphorus from  
628 the water column to the sediments. Following dissolution of solid Fe minerals in the  
629 sediments, the adsorbed P is released to the porewaters. However, in the Peruvian OMZ,  
630 oxygen concentrations in the water column are generally below detection limit. Consequently,  
631 Fe (oxyhydr)oxides are likely already dissolved in the water column and not such an  
632 important P source to the sediments. An estimate of phosphate released during the reduction  
633 of Fe (oxyhydr)oxides can be calculated from the diffusive  $\text{Fe}^{2+}$  fluxes and the molar Fe/P  
634 ratio typically found in Fe (oxyhydr)oxides. The diffusive  $\text{Fe}^{2+}$  fluxes were in the range of 0  
635 to  $0.03 \text{ mmol m}^{-2} \text{ d}^{-1}$  during the M92 cruise (Table 4) and the molar Fe/P ratio of Fe  
636 (oxyhydr)oxides in the sediments is around 10 [Slomp et al., 1996]. The calculation of the  
637  $\text{TPO}_4$  release rates from Fe (oxyhydr)oxides (Eq. 14 in Table 2) results in a flux of  $0.003$   
638  $\text{mmol PO}_4^{3-} \text{ m}^{-2} \text{ d}^{-1}$  (Table 4, Fig. 4C and 5B), which is equivalent to less than 5% of the  
639 benthic P flux and burial flux.

640 An additional internally activated P pool is phosphate released from large sulfur-oxidizing  
641 bacteria, e.g. *Beggiatoa* [Sannigrahi and Ingall, 2005; Brock and Schulz-Vogt, 2011]. These  
642 microorganisms store P in the form of intracellular polyphosphate granules when terminal  
643 electron acceptors for sulfide oxidation are available (oxic conditions) and release dissolved P  
644 during periods when these oxidants are scarce (anoxic conditions). Hence, it is generally  
645 assumed that they strongly affect benthic TPO<sub>4</sub> fluxes in a system with frequently changing  
646 bottom water redox conditions [Ingall and Jahnke, 1994; Sannigrahi and Ingall, 2005; Schulz  
647 and Jørgensen, 2005; Brock and Schulz-Vogt, 2011; Dale et al., 2013]. Polyphosphates have  
648 been shown to be an important P pool in the sediments of highly productive upwelling areas  
649 [Kraal et al., 2015]. Along the depth transect at Peru, dense mats of sulfur bacteria related to  
650 *Marithioploca* were observed on the sediments during video-launched MUC and benthic  
651 lander deployments down to 300 m water depth [Dale et al., 2015]. Similar findings extended  
652 distributions of microbial mats along a latitudinal transect at 11°S off were also previously  
653 described by Mosch et al. (2012) and Gutiérrez et al. (2008). Although, these organisms are  
654 not known to store polyphosphates like their close relatives, *Beggiatoa* spp. and  
655 *Thiomargarita* spp. [Høgslund et al., 2009; Holmkvist et al., 2010], our findings provide  
656 circumstantial indications for P uptake and release by *Marithioploca*-related bacteria.

657 Firstly, we found that the relative abundance of copies of *Marithioploca*-related bacteria per g<sup>-1</sup>  
658 sediment and the measured benthic TPO<sub>4</sub> release rates correlate linearly ( $r^2=0.92$ , Fig. 6).  
659 This finding supports the suggestion that bacteria exert an important control on benthic P  
660 fluxes. Secondly, a comparison of the in situ measured benthic P fluxes and the diffusive P  
661 fluxes calculated from the difference of the TPO<sub>4</sub> bottom water concentration and the TPO<sub>4</sub>  
662 porewater concentration of the surface sediments revealed large differences (Fig. 4B). Such a  
663 difference could be explained by the lysis of bacterial cells during sample retrieval followed  
664 by the release of the internally stored polyphosphate pool into the porewater. Following this  
665 argument, the diffusive P fluxes cannot be taken as real fluxes, but as a measure for potential  
666 maximum release rates of P by *Marithioploca*-related bacteria. It should be noted that, the  
667 potential fluxes are more than sufficient to compensate for the missing P fraction in transect  
668 section II (ranging from 0.5 to 1.6 mmol m<sup>-2</sup> d<sup>-1</sup>; Table 4, Fig. 4B).

669 In addition to the established porewater extraction procedure, we carried out freeze/thaw  
670 experiments to quantify the amount of P stored in sulfide-oxidizing bacteria (see method  
671 section 3.7). The released polyphosphates from the microbial cells after repeated freeze/thaw

672 cycles are rapidly hydrolyzed to orthophosphate under acidic conditions [Jager and Heyns,  
673 1998]. Hence, the standard method to determine phosphate in the porewaters using acidic  
674 reagents will favor the hydrolysis of polyphosphates enabling us to measure its concentration  
675 in the porewaters after conducting the experiments. However, this method cannot exclude P  
676 release from other bacteria and, possibly, foraminifera in the sediments. A comparison of the  
677 porewater phosphate concentrations and the experiment results shows that the internal P  
678 reservoir is as twice as high as the porewater P concentration in transect section I and more  
679 than ten times larger in section II (Fig. 7). These results are coincident with the findings from  
680 the mass balance approach, where the largest discrepancies occur in transect section II and are  
681 another indication for the bacterial impact on the benthic P release. Interestingly, the highest  
682 phosphate concentrations after the freeze/thaw experiments were found at station VIII (407  
683 m) with abundant foraminifera rather than sulfide-oxidizing bacteria. Hence, we assume that  
684 the sulfide-oxidizing bacteria at station IV, V and VI (141, 194 and 244 m) and, potentially,  
685 the foraminifera observed at station VIII (407 m) are contributing phosphate to the  
686 porewaters. To our knowledge, P storage by foraminifera has not been demonstrated  
687 previously and awaits further study.

688 It remains to be shown how these mechanisms play out in detail (e.g. nutrient concentration  
689 thresholds, P uptake and release time scales by *Marithioploca*-related bacteria) and how they  
690 impact benthic P release in oxygen and nitrate deficient environments on longer time scales.  
691 Summarizing the results of the mass balance, it should be noted, that, even with the relevant  
692 data on particulate P rain rates, the benthic P mass balance for the core of the Peruvian OMZ  
693 is imbalanced and requires an additional P source to maintain the benthic  $\text{TPO}_4$  fluxes. We  
694 suggest that sulfur bacteria make important contribution to this missing P source.

### 695 **5.2.3 Indications for active phosphorite formation**

696 In contrast to the stations between 74 and 244 m water depth characterized by P release, data  
697 from station VIII at 407 m water depth indicate the uptake of phosphate from the bottom  
698 water. To our best knowledge, this is the first time that a downward flux of dissolved  
699 phosphate from bottom waters into phosphorite-bearing surface sediments has been  
700 documented by in situ benthic flux measurements. Furthermore, the PIP concentrations in the  
701 surface sediments of station VIII (Fig. 2A) were 10 to 60 times higher compared to the  
702 shallower stations where P was released from the sediments. Taken together, these



703 observations indicate that a PIP phase, likely phosphorite, was precipitating from the  
704 porewater phosphate at the time of sampling. This is also reflected in decreasing porewater  
705 phosphate concentrations (Fig. 7).

706 Arning et al. (2008) presented investigations on phosphorites recovered from the Peruvian  
707 OMZ including a station at 12°S from the same water depth (~ 400 m) close to sampling  
708 station VIII. The suboxic bottom waters and low sedimentation rates in that area seem to be  
709 favorable for phosphorite formation close to the sediment-water interface [Arning et al.,  
710 2009b]. Cosmidis et al. (2013) suggested three mechanisms how high porewater phosphate  
711 concentrations that are essential for the phosphogenesis can be generated in the sediments: (1)  
712 remineralization of organic matter mainly through bacterial sulfate reduction releasing  
713 phosphate to the porewaters, (2) reductive dissolution of Fe (oxyhydr)oxides and the release  
714 of adsorbed P and (3) synthesis of internally stored polyphosphates by large sulfide-oxidizing  
715 bacteria. Using the same mass balance approach as presented before, we calculated a P  
716 accumulation rate of  $33 \pm 4 \text{ mmol m}^{-2} \text{ yr}^{-1}$  at station VIII where most of the P is derived from  
717 ambient bottom waters ( $26 \text{ mmol m}^{-2} \text{ yr}^{-1}$ ). Hence, our data suggest that the phosphorite  
718 nodules at this station contain phosphate that originates predominantly from ambient bottom  
719 waters. Additionally, as already mentioned, sediments at station VIII were covered by benthic  
720 foraminifera instead of mat-forming sulfur bacteria. The release of phosphate from frozen  
721 samples from this site may indicate that these foraminifera are a source for polyphosphates  
722 (see section 3.7 and Fig. 7). Our observations suggest that benthic foraminifera rather than  
723 bacterial mats might facilitate the uptake of bottom water phosphate and the formation of  
724 phosphorites at this station. However, this remains an open question and should be addressed  
725 in future field campaigns.

726 The P uptake rate of  $\sim 26 \text{ mmol P m}^{-2} \text{ yr}^{-1}$  derived from our lander measurements may be  
727 compared to previous estimates on phosphorite growth rates in the area. Dating of phosphoric  
728 laminites yields a P uptake rate of only  $3 \text{ mmol P m}^{-2} \text{ yr}^{-1}$  for a ca. 1 Ma old nodule [Arning et  
729 al., 2009a]. These different fluxes may be at least partly explained by the methodological  
730 difference (present flux measurement vs. long-term average). However, growth rates  
731 determined on modern nodules are broadly consistent with our flux measurements [Burnett et  
732 al., 1982].

733

## 734 **6 Conclusions**

735 This study aimed to identify the P sources of benthic P release in the Peruvian OMZ. We  
736 determined the rain rates of particulate organic phosphorus and particulate inorganic  
737 phosphorus as well as benthic P release rates and P burial fluxes.

738 Our calculations revealed that within the core OMZ particulate phosphorus rain rates cannot  
739 account for measured benthic P fluxes and burial fluxes. From systematic analysis of potential  
740 P sources, we conclude that periodic P release from sulfur bacteria that store and release P  
741 under oscillating redox conditions could strongly modulate benthic P fluxes, and hence  
742 explain the missing P source. We visited the area during austral summer when oxygen and  
743 nitrate levels were depleted by high export production and respiration. It is possible that the  
744 Peruvian OMZ was less reducing prior to our sampling period due to lower respiration rates  
745 and/or better ventilation. Thus, we propose that the bacterial mats on the Peru margin act as  
746 phosphorus capacitors, being discharged during austral summer and recharged during other  
747 periods of the year when bottom waters are less reducing, as previously proposed in Dale et  
748 al. (2013). This hypothesis could be tested by studying of the seasonality of benthic fluxes in  
749 the Peruvian up-welling system and P dynamics within the bacterial community.

750 In addition, measurements at one station (407 m water depth) showed clear indications for the  
751 uptake of dissolved phosphate by the sediments facilitating phosphorite formation. Our data  
752 imply that most of the P accumulating in these authigenic minerals originates from ambient  
753 bottom waters. Since this site was marked by a high abundance of P-bearing benthic  
754 foraminifera, we speculate that phosphate uptake and phosphorite formation may be linked to  
755 the presence of these organisms. This requires further study.

756 There was no clear preferential mineralization of POP relative to POC with depth in the water  
757 column. POC/TPP ratios in both water column particles and sediments were close to Redfield  
758 at most sites in the Peruvian OMZ. This observation strongly suggests that the relative burial  
759 efficiencies of POC and TPP are similar under low oxygen conditions. Importantly, it further  
760 shows that the sediments underlying the anoxic waters on the Peru margin are not depleted in  
761 P compared to Redfield. Rather, they are depleted relative to sediments underlying oxic  
762 waters, which show POC/TPP ratios well below Redfield (Wallmann, 2010). Thus, at Peru, a  
763 lack of oxygen promotes the intensified release of dissolved P from sediments, whilst  
764 preserving a POC/TPP burial ratio that is similar to Redfield.

765 Our data support the hypothesis that benthic P release is linked via a positive feedback loop to  
766 intensified primary production in the surface water and oxygen demand in the water column  
767 during periods where bottom waters redox conditions promote the release of P from the  
768 sediments. However, this positive feedback is limited by the formation of authigenic  
769 inorganic P phases that maintains the long-term average POC/TPP burial ratio close to  
770 Redfield.

771

#### 772 **Author contribution**

773 UL, AD and SS supported the shipboard work, geochemical analysis and contributed to the  
774 manuscript. CH, KW and AN helped with fruitful discussions related to the manuscript and  
775 with the manuscript preparation. CL carried out the molecular analysis and contributed to the  
776 manuscript.

777

#### 778 **Acknowledgements**

779 We are very grateful to the crew of RV *Meteor* during cruise M92 for the support of. Our  
780 thanks also go to A. Petersen, M. Türk and S. Cherednichenko for their assistance in  
781 deploying the landers. For their enthusiastic help and cooperation, we thank B. Domeyer, S.  
782 Kriwanek, A. Bleyer, R. Suhrberg, S. Trinkler and V. Thoenissen for biogeochemical  
783 analyses on board and in the home laboratory. Furthermore, we appreciate Christopher Voigt  
784 from the University of Bremen for carrying out XRD analysis. This work is a contribution of  
785 the Sonderforschungsbereich 754 “Climate – Biogeochemistry Interactions in the Tropical  
786 Ocean” ([www.sfb754.de](http://www.sfb754.de)) which is supported by the Deutsche Forschungsgemeinschaft.

787

788 **References**

- 789 Anderson, L. D., Delaney, M. L., and Faul, K. L.: Carbon to phosphorus ratios in sediments:  
790 Implications for nutrient cycling, *Global Biogeochemical Cycles*, 15(1), 65-79, 2001.
- 791 Arning, E. T., Birgel, D., Schulz-Vogt, H. N., Holmkvist, L., Jørgensen, B. B., Larson, A.,  
792 and Peckmann, J.: Lipid Biomarker Patterns of Phosphogenic Sediments from Upwelling  
793 Regions, *Geomicrobiology Journal*, 25(2), 69-82, 2008.
- 794 Arning, E. T., Birgel, D., Brunner, B., and Peckmann, J.: Bacterial formation of phosphatic  
795 laminites off Peru, *Geobiology*, 7(3), 295-307, 2009a.
- 796 Arning, E. T., Lückge, A., Breuer, C., Gussone, N., Birgel, D., and Peckmann, J.: Genesis of  
797 phosphorite crusts off Peru, *Marine Geology*, 262(1-4), 68-81, 2009b.
- 798 Asahi, T., Ichimi, K., Yamaguchi, H., and Tada, K.: Horizontal distribution of particulate  
799 matter and its characterization using phosphorus as an indicator in surface coastal water,  
800 Harima-Nada, the Seto Inland Sea, Japan, *Journal of Oceanography*, 70(3), 277-287, 2014.
- 801 Aspila, K. I., Agemian, H., and Chau, A. S. Y.: A semi-automated Method for the  
802 Determination of Inorganic, Organic and Total Phosphate in Sediments, *Analyst*, 101, 187-  
803 197, 1976.
- 804 Baturin, G. N.: Issue of the relationship between primary productivity of organic carbon in  
805 ocean and phosphate accumulation (Holocene– Late Jurassic), *Lithol. Miner. Resour.*, 42(4),  
806 318–348, 2007, doi:10.1134/ S0024490207040025.
- 807 Benitez-Nelson, C. R.: The biogeochemical cycling of phosphorus in marine systems, *Earth-*  
808 *Science Reviews*, 51(1-4), 109-135, 2000.
- 809 Benitez-Nelson, C. R., O'Neill, L., Kolowith, L. C., Pellechia, P., and Thunell, R.:  
810 Phosphonates and particulate organic phosphorus cycling in an anoxic marine basin, *Limnol.*  
811 *Ocean.*, 49(5), 1593-1604, 2004.
- 812 Benitez-Nelson, C. R., O'Neill Madden, L. P., Styles, R. M., Thunell, R. C., and Astor, Y.:  
813 Inorganic and organic sinking particulate phosphorus fluxes across the oxic/anoxic water  
814 column of Cariaco Basin, Venezuela, *Marine Chemistry*, 105(1-2), 90-100, 2007.

815 Berelson, W. M., Hammond, D. E., and Johnson, K. S.: Benthic fluxes and the cycling of  
816 biogenic silica and carbon in two southern California borderland basins, *Geochimica et*  
817 *Cosmochimica Acta*, 51(6), 1345-1363, 1987.

818 Berelson, W., McManus, J., Coale, K., Johnson, K., Burdige D., Kilgore, T., Colodner, D.,  
819 Chavez, F., Kudela, R., and Boucher, J.: A time series of benthic flux measurements from  
820 Monterey Bay, CA, *Continental Shelf Research*, 23(5), 457-481, 2003.

821 Bertics, V. J., Löscher, C. R., Salonen, I., Dale, A. W., Gier, J., Schmitz, R. A. and Treude,  
822 T.: Occurrence of benthic microbial nitrogen fixation coupled to sulfate reduction in the  
823 seasonally hypoxic Eckernförde Bay. Baltic Sea. *Biogeosciences*. 10, 1243-1258, 2013.

824 Boudreau, B. P.: The diffusive tortuosity of fine-grained unlithified sediments. *Geochim.*  
825 *Cosmochim. Acta* 60, 3139–3142, 1996.

826 Brock, J., and Schulz-Vogt, H. N.: Sulfide induces phosphate release from polyphosphate in  
827 cultures of a marine *Beggiatoa* strain, *ISME J*, 5(3), 497-506, 2011.

828 Burnett, W. C., Beers, M. J., and Roe, K. K.: Growth Rates of Phosphate Nodules from the  
829 Continental Margin Off Peru, *Science*, 215(4540), 1616-1618, 1982.

830 Colman, A. S., Mackenzie, F. T., & Holland, H. D. Redox Stabilization of the Atmosphere  
831 and Oceans and Marine Productivity. *Science* 275, 406-408. 1997.

832 Compton, J., Mallinson, D., Glenn, C., Filipelli, G., Föllmi, K., Shields, G., and Zanin, Y.:  
833 Variations in the global phosphorus cycle, in *Marine authigenesis: from global to microbial*,  
834 *SEPM (Society for Sedimentary Geology)*, 21-33, 2000.

835 Cosmidis, J., Benzerara, K., Menguy, N., and Arning, E.: Microscopy evidence of bacterial  
836 microfossils in phosphorite crusts of the Peruvian shelf: Implications for phosphogenesis  
837 mechanisms, *Chemical Geology*, 359, 10-22, 2013.

838 Dale, A., Bertics, W., V. J., Treude, T., Sommer, S., and Wallmann, K. Modeling benthic–  
839 pelagic nutrient exchange processes and porewater distributions in a seasonally hypoxic  
840 sediment: evidence for massive phosphate release by *Beggiatoa*? *Biogeosciences* 10, 629-651,  
841 2003.

842 Dale, A. W., Sommer, S., Lomnitz, U., Montes, I., Treude, T., Liebetrau, V., Gier, J., Hensen,  
843 C., Dengler, M., Stolpovsky, K., Bryant, L. D., and Wallmann, K.: Organic carbon  
844 production, mineralisation and preservation on the Peruvian margin, *Biogeosciences*, 12(5),  
845 1537-1559, 2015.

846 Delaney, M. L.: Phosphorus accumulation in marine sediments and the oceanic phosphorus  
847 cycle, *Global Biogeochemical Cycles*, 12(4), 563-572, 1998.

848 Díaz-Ochoa, J. A., Lange, C. B., Pantoja, S., De Lange, G. J., Gutierrez, D., Munoz, P., and  
849 Salamanca M.: Fish scales in sediments from off Callao, central Peru, *Deep-Sea Res. Part II-*  
850 *Top. Stud. Oceanogr.*, 56(16), 1113-1124, 2009.

851 Faul, K. L., Paytan, A., and Delaney, M. L.: Phosphorus distribution in sinking oceanic  
852 particulate matter, *Marine Chemistry*, 97(3-4), 307-333, 2005.

853 Filippelli, G. M.: Controls on phosphorus concentration and accumulation in oceanic  
854 sediments, *Marine Geology*, 139(1-4), 231-240, 1997.

855 Filippelli, G. M.: The global phosphorus cycle, in *Phosphates: Geochemical, Geobiological,*  
856 *and Materials Importance*, edited by M. Kohn, J. Rakovan and J. Hughes, pp. 391-425,  
857 *Reviews in Mineralogy&Geochemistry*, 2002.

858 Filippelli, G. M. (2008), *The Global Phosphorus Cycle: Past, Present, and Future*, *Elements*,  
859 4(2), 89-95.

860 Föllmi, K. B.: The phosphorus cycle, phosphogenesis and marine phosphate-rich deposits,  
861 *Earth-Science Reviews*, 40(1-2), 55-124, 1996.

862 Franz, J., Krahnemann, G., Lavik, G., Grasse, P., Dittmar, T., and Riebesell, U.: Dynamics and  
863 stoichiometry of nutrients and phytoplankton in waters influenced by the oxygen minimum  
864 zone in the eastern tropical Pacific, *Deep Sea Research Part I: Oceanographic Research*  
865 *Papers*, 62(0), 20-31, 2012.

866 Froelich, P. N., Arthur, M. A., Burnett, W. C., Deakin, M., Hensley, V., Jahnke, R., Kaul, L.,  
867 Kim, K. H., Roe, K., Soutar, A., Vathakanon, C.: Early diagenesis of organic matter in Peru  
868 continental margin sediments: Phosphorite precipitation, *Marine Geology*, 80(3-4), 309-343,  
869 1988.

870 Fuenzalida, R., Schneider, W., Garcés-Vargas, J., Bravo, L., and Lange, C.: Vertical and  
871 horizontal extension of the oxygen minimum zone in the eastern South Pacific Ocean, *Deep*  
872 *Sea Research Part II: Topical Studies in Oceanography*, 56(16), 992-1003, 2009.

873 Ganeshram, R. S., Pedersen, T. F., Calvert, S., and Francois, R.: Reduced nitrogen fixation in  
874 the glacial ocean inferred from changes in marine nitrogen and phosphorus inventories,  
875 *Nature*, 415(6868), 156-159, 2002.

876 Glenn, C. R., and Arthur, M. A.: Petrology and major element geochemistry of Peru margin  
877 phosphorites and associated diagenetic minerals: Authigenesis in modern organic-rich  
878 sediments, *Marine Geology*, 80(3-4), 231-267, 1988.

879 Goldhammer, T., Bruchert, V., Ferdelman, T. G., and Zabel, M.: Microbial sequestration of  
880 phosphorus in anoxic upwelling sediments, *Nature Geosci*, 3(8), 557-561, 2010.

881 Govindaraju K.: Compilation of working values and sample description for 383 geostandards.  
882 *Geostandard Newslett.* 18, 1-158, 1994.

883 Graco, M., Purca, S., Dewitte, B., Morón, O., Ledesma, J., Flores, G., Castro, C., and  
884 Gutiérrez, D.: The OMZ and nutrients features as a signature of interannual and low  
885 frequency variability off the peruvian upwelling system, *Biogeosciences Discuss.*, 2016, 1-36,  
886 2016.

887 Grasshoff, K., Erhardt, M., Kremling, K.: *Methods of seawater analysis*, 3rd ed. Wiley-VCH  
888 (1999).

889 Gutiérrez, D., Enríquez, E., Purca, S., Quipúzcoa, L., Marquina, R., Flores, G., and Graco,  
890 M.: Oxygenation episodes on the continental shelf of central Peru: Remote forcing and  
891 benthic ecosystem response, *Progress in Oceanography*, 79(2-4), 177-189, 2008.

892 Hedges, J. I., Hu, F. S., Devol, A. H., Hartnett H. E., Tsamakis, E., & Keil, R. G.:  
893 Sedimentary organic matter preservation: A test for selective degradation under oxic  
894 conditions. *American Journal of Science* 299, 529-555. 1999.

895 Høglund, S., Revsbech, N. P., Kuenen, J. G., Jørgensen, B. B., Gallardo, V. A., Vossenberg,  
896 J. v. d., Nielsen, J. L., Holmkvist, L., Arning, E. T., and Nielsen, L. P.: Physiology and  
897 behaviour of marine *Thioploca*, *ISME J*, 3(6), 647-657, 2009.

- 898 Holmkvist, L., Arning, E. T., Küster-Heins, K., Vandieken, V., Peckmann, J., Zabel, M., and  
899 Jørgensen, B. B.: Phosphate geochemistry, mineralization processes, and Thioploca  
900 distribution in shelf sediments off central Chile, *Marine Geology*, 277(1–4), 61-72, 2010.
- 901 Ingall, E. D., and Van Cappellen P.: Relation between sedimentation rate and burial of  
902 organic phosphorus and organic carbon in marine sediments, *Geochimica et Cosmochimica*  
903 *Acta*, 54(2), 373-386, 1990.
- 904 Ingall, E. D., Bustin, R. M., and Van Cappellen, P.: Influence of water column anoxia on the  
905 burial and preservation of carbon and phosphorus in marine shales, *Geochimica et*  
906 *Cosmochimica Acta*, 57(2), 303-316, 1993.
- 907 Ingall, E., and Jahnke R.: Evidence for enhanced phosphorus regeneration from marine  
908 sediments overlain by oxygen depleted waters, *Geochimica et Cosmochimica Acta*, 58(11),  
909 2571-2575, 1994
- 910 Ingall, E., Kolowith, L., Lyons, T., and Hurtgen, M.: Sediment carbon, nitrogen and  
911 phosphorus cycling in an anoxic fjord, Effingham Inlet, British Columbia, *American Journal*  
912 *of Science*, 305(3), 240-258, 2005.
- 913 Ingall, E. D.: Biogeochemistry: Phosphorus burial, *Nature Geosci*, 3(8), 521-522, 2010.
- 914 de Jager, H.-J., and Heyns, A. M.: Kinetics of Acid-Catalyzed Hydrolysis of a Polyphosphate  
915 in Water, *The Journal of Physical Chemistry A*, 102(17), 2838-2841, 1998.
- 916 Jahnke, R. A.: Early diagenesis and recycling of biogenic debris at the seafloor, Santa Monica  
917 Basin, California, *Journal of Marine Research*, 48(2), 413-436, 1990.
- 918 Jilbert, T., Slomp, C. P., Gustafsson, B. G., and Boer W.: Beyond the Fe-P-redox connection:  
919 preferential regeneration of phosphorus from organic matter as a key control on Baltic Sea  
920 nutrient cycles, *Biogeosciences*, 8(6), 1699-1720, 2011.
- 921 Kraal, P., Slomp, C. P., Reed, D. C, Reichart, G.-J., and Poulton, S. W.: Sedimentary  
922 phosphorus and iron cycling in and below the oxygen minimum zone of the northern Arabian  
923 Sea, *Biogeosciences*, 9(7), 2603-2624, 2012.



- 924 Kraal, P., Bostick, B. C., Behrends, T., Reichart, G.-J., and Slomp, C. P.: Characterization of  
925 phosphorus species in sediments from the Arabian Sea oxygen minimum zone: Combining  
926 sequential extractions and X-ray spectroscopy, *Marine Chemistry*, 168(0), 1-8, 2015.
- 927 Krissek, L. A., Scheidegger, K. F., and Kulm, L. D.: Surface sediments of the Peru-Chile  
928 continental margin and the Nazca plate, *Geological Society of America Bulletin*, 91(6), 321-  
929 331, 1980.
- 930 Li, Y.-H. and Gregory, S.: Diffusion of ions in sea water and in deep-sea sediments. *Geochim.*  
931 *Cosmochim. Acta* 38, 703–714, 1974.
- 932 Loh, A. N., and Bauer, J. E.: Distribution, partitioning and fluxes of dissolved and particulate  
933 organic C, N and P in the eastern North Pacific and Southern Oceans, *Deep Sea Research Part*  
934 *I: Oceanographic Research Papers*, 47(12), 2287-2316, 2000.
- 935 Löscher, C. R., Kock, A., Könneke, M., LaRoche, J., Bange, H. W., and Schmitz, R. A.:  
936 Production of oceanic nitrous oxide by ammonia-oxidizing archaea. *Biogeosciences*. 9. 2419-  
937 2429, 2012.
- 938 Lyons, G., Benitez-Nelson, C. R., and Thunell, R. C.: Phosphorus composition of sinking  
939 particles in the Guaymas Basin, Gulf of California, *Limnology and Oceanography*, 56(3),  
940 1093-1105, 2011.
- 941 McManus, J., Berelson, W. M., Coale, K. H., Johnson, K. S., and Kilgore, T. E.: Phosphorus  
942 regeneration in continental margin sediments, *Geochimica et Cosmochimica Acta*, 61(14),  
943 2891-2907, 1997.
- 944 Mort, H. P., C. P. Slomp, B. G. Gustafsson, and T. J. Andersen (2010), Phosphorus recycling  
945 and burial in Baltic Sea sediments with contrasting redox conditions, *Geochimica et*  
946 *Cosmochimica Acta*, 74(4), 1350-1362.
- 947 Mosch, T., Sommer, S., Dengler, M., Noffke, A., Bohlen, L., Pfannkuche, O., Liebetrau, V.,  
948 and Wallmann, K.: Factors influencing the distribution of epibenthic megafauna across the  
949 Peruvian oxygen minimum zone, *Deep Sea Research Part I: Oceanographic Research Papers*,  
950 68(0), 123-135, 2012.

951 Noffke A., Hensen, C., Sommer, S., Scholz, F., Bohlen L., Mosch, T., Graco M., and  
952 Wallmann K.: Benthic iron and phosphorus fluxes across the Peruvian oxygen minimum  
953 zone, *Limnology and Oceanography*, 57(3), 851-867, 2012.

954 Noffke A., Phosphorus cycling in anoxic sediments, PhD dissertation, University of Kiel,  
955 2014.

956 Noffke, A., Sommer, S., Dale, A.W., Hall, P.O.J., Pfannkuche, O.: Benthic nutrient fluxes in  
957 the Eastern Gotland Basin (Baltic Sea) with particular focus on microbial mat ecosystems,  
958 *Journal of Marine Systems*, 2016, doi: 10.1016/j.jmarsys.2016.01.007.

959 Paytan, A., Cade-Menun, B. J., McLaughlin, K., and Faul, K. L.: Selective phosphorus  
960 regeneration of sinking marine particles: evidence from <sup>31</sup>P-NMR, *Marine Chemistry*, 82(1–  
961 2), 55-70, 2003.

962 Paytan, A., and McLaughlin, K.: The Oceanic Phosphorus Cycle, *Chemical Reviews*, 107(2),  
963 563-576, 2007.

964 Pennington, J. T., Mahoney, K. L., Kuwahara, V. S., Kolber, D. D., Calienes, R., and Chavez,  
965 F. P.: Primary production in the eastern tropical Pacific: A review, *Progress in Oceanography*,  
966 69(2–4), 285-317, 2006.

967 Redfield, A. C., Ketchum, B. H., and Richards, F. A.: The influence of organisms on the  
968 composition of seawater, in *The Sea*, Academic Press, London, 26-77, 1963.

969 Reimers, C. E., and Suess, E.: Spatial and temporal patterns of organic matter accumulation  
970 on the Peru continental margin, in *Coastal Upwelling: Part B. Sedimentary Record of Ancient*  
971 *Coastal Upwelling*, edited by E. Suess and J. Thiede, pp. 311-346, Plenum Press, New York,  
972 1983.

973 Roth, R., S. P. Ritz, S. P. and Joos, F.: Burial-nutrient feedbacks amplify the sensitivity of  
974 atmospheric carbon dioxide to changes in organic matter remineralisation. *Earth Syst.*  
975 *Dynam.*, 5, 321-343, 2014, doi:10.5194/esd-5-321-2014.

976 Ruttenger, K. C., and Berner, R. A.: Authigenic apatite formation and burial in sediments  
977 from non-upwelling, continental margin environments, *Geochimica et Cosmochimica Acta*,  
978 57(5), 991-1007, 1993.

979 Ruttenberg, K. C.: The Global Phosphorus Cycle, In: Turekian KK, Holland DJ, editors.  
980 Treatise on Geochemistry. Elsevier, 585–643, 2003.

981 Ruttenberg, K. C.: The Global Phosphorus Cycle. In Treatise on Geochemistry Volume 10, H.  
982 D. Holland and K. K. Turekian (eds), Elsevier, p 499-558. 2014.

983 Salman, V., Amann, R, Shub, D. A., Schulz-Vogt, H. N.: Multiple self-splicing introns in the  
984 16S rRNA genes of giant sulfur bacteria, PNAS, 109(11), 4203-4208, 2012,  
985 doi:10.1073/pnas.1120192109.

986 Salman, V., Amann R., Girth A.-C., Polerecky L., Bailey J. V., Høglund S., Jessen G.,  
987 Pantoja S., and Schulz-Vogt H. N.: A single-cell sequencing approach to the classification of  
988 large, vacuolated sulfur bacteria, *Systematic and Applied Microbiology*, 34(4), 243-259, 2011.

989 Sannigrahi, P., and Ingall, E.: Polyphosphates as a source of enhanced P fluxes in marine  
990 sediments overlain by anoxic waters: Evidence from 31P NMR, *Geochemical Transactions*,  
991 6(3), 52, 2005.

992 Sanudo-Wilhelmy, S. A., Tovar-Sanchez, A., Fu, F.-X., Capone, D. G., Carpenter, E. J., and  
993 Hutchins, D. A.: The impact of surface-adsorbed phosphorus on phytoplankton Redfield  
994 stoichiometry, *Nature*, 432(7019), 897-901, 2004

995 Schenau, S. J., and De Lange, G. J.: A novel chemical method to quantify fish debris in  
996 marine sediments, *Limnology and Oceanography*, 45(4), 963-971, 2000.

997 Schenau, S. J., and De Lange, G. J.: Phosphorus regeneration vs. burial in sediments of the  
998 Arabian Sea, *Marine Chemistry*, 75(3), 201-217, 2001.

999 Scholz, F., C. Hensen, A. Noffke, A. Rohde, V. Liebetrau, and K. Wallmann (2011), Early  
1000 diagenesis of redox-sensitive trace metals in the Peru upwelling area – response to ENSO-  
1001 related oxygen fluctuations in the water column, *Geochimica et Cosmochimica Acta*, 75(22),  
1002 7257-7276.

1003 Schulz, H. N. and Jørgensen, B. B.: Thiomargarita, In Krieg, N. R., J. T. Staley, and D. J.  
1004 Brenner (ed), *Bergey's Manual of Determinative Bacteriology*, Vol. 2, part B, Springer-  
1005 Verlag, Berlin, Heidelberg, New York, 2005.

- 1006 Schulz, H. N., and Schulz, H. D.: Large Sulfur Bacteria and the Formation of Phosphorite,  
1007 Science, 307(5708), 416-418, 2005.
- 1008 Schunck, H., Lavik, G., Desai, D. K., Großkopf, T., Kalvelage, T., Löscher, C. R., Paulmier,  
1009 A., Contreras, S., Siegel, H., Holtappels, M., Rosenstiel, P., Schilhabel, M. B., Graco, M.,  
1010 Schmitz, R. A., Kuypers, M. M. M., LaRoche, J.: Giant Hydrogen Sulfide Plume in the  
1011 Oxygen Minimum Zone off Peru Supports Chemolithoautotrophy, PLoS ONE 8(8), 2013.
- 1012 Sekula-Wood, E., Benitez-Nelson, C. R., Bennett, M. A., and Thunell R.: Magnitude and  
1013 composition of sinking particulate phosphorus fluxes in Santa Barbara Basin, California,  
1014 Global Biogeochemical Cycles, 26(2), GB2023, 2012.
- 1015 Slomp, C. P., Van der Gaast, S. J., and Van Raaphorst, W.: Phosphorus binding by poorly  
1016 crystalline iron oxides in North Sea sediments, Marine Chemistry, 52(1), 55-73, 1996.
- 1017 Slomp, C. P., Malschaert, J. F. P., and Van Raaphorst, W.: The role of adsorption in  
1018 sediment-water exchange of phosphate in North Sea continental margin sediments, Limnol.  
1019 Ocean., 43(5), 832-846, 1998.
- 1020 Slomp, C. P., and Van Cappellen, P.: The global marine phosphorus cycle: sensitivity to  
1021 oceanic circulation, Biogeosciences, 4(2), 155-171, 2007.
- 1022 Sommer, S., Linke, P., Pfannkuche, O., Schleicher, T., v. Deimling, S., Reitz, A., Haeckel,  
1023 M., and Hensen, C.: Seabed methane emissions and the habitat of frenulate tubeworms on the  
1024 Captain Arutyunov mud volcano (Gulf of Cadiz), Marine Ecology Progress Series, 382, 69-  
1025 86, 2009.
- 1026 Sommer, S., Gier, J., Treude, T., Lomnitz, U., Dengler, M., Cardich, J. and Dale, A.:  
1027 Depletion of oxygen, nitrate and nitrite in the Peruvian oxygen minimum zone cause an  
1028 imbalance of benthic nitrogen fluxes. Deep-Sea Research Part I, in review, 2015.
- 1029 Stramma, L., Johnson, G. C., Sprintall, J., and Mohrholz, V.: Expanding Oxygen-Minimum  
1030 Zones in the Tropical Oceans, Science, 320(5876), 655-658, 2008.
- 1031 Strub, P. T., Mesias, J. M., Montecino, V., Ontecino, R., and Salinas S.: Coastal ocean  
1032 circulation of western South. America, in The Sea, edited by A. R. R. a. K. H. Brink, pp. 273-  
1033 313, Wiley, 1998.

- 1034 Suess, E.: Phosphate regeneration from sediments of the Peru continental margin by  
1035 dissolution of fish debris, *Geochimica et Cosmochimica Acta*, 45(4), 577-588, 1981.
- 1036 Suess, E., Kulm, L. D., and Killingley, J. S.: Coastal upwelling and a history of organic rich  
1037 mudstone deposition off Peru., in *Marine Petroleum Source rocks*, edited by J. Brooks and A.  
1038 J. Fleet, pp. 1129-1145, Geological Society Spec, 1987.
- 1039 Suess, E., and von Huene, R.: Ocean Drilling Program Leg 112, Peru continental margin: Part  
1040 2, Sedimentary history and diagenesis in a coastal upwelling environment, *Geology*, 16(10),  
1041 939-943, 1988.
- 1042 Sundby, B., Anderson, L. G., Hall, P. O. J., Iverfeldt, Å., van der Loeff, M. M. R., and  
1043 Westerlund, S. F. G.: The effect of oxygen on release and uptake of cobalt, manganese, iron  
1044 and phosphate at the sediment-water interface, *Geochimica et Cosmochimica Acta*, 50(6),  
1045 1281-1288, 1986.
- 1046 Tamura K., Stecher, G., Peterson, D., Filipski, A. and Kumar, S.: MEGA6, Molecular  
1047 Evolutionary Genetics Analysis Version 6.0. *Molecular Biology and Evolution* 30: 2725-  
1048 2729, 2013.
- 1049 Teske, A., Ramsing, N. B., Küver, J., and Fossing, H.: Phylogeny of Thioploca and Related  
1050 Filamentous Sulfide-Oxidizing Bacteria, *Systematic and Applied Microbiology*, 18(4), 517-  
1051 526, 1995.
- 1052 Tsandev, I., Reed, D. C., and Slomp, C. P.: Phosphorus diagenesis in deep-sea sediments:  
1053 Sensitivity to water column conditions and global scale implications, *Chemical Geology*,  
1054 330–331(0), 127-139, 2012.
- 1055 Van Cappellen, P., and Ingall, E. D.: Redox Stabilization of the Atmosphere and Oceans by  
1056 Phosphorus-Limited Marine Productivity, *Science*, 271(5248), 493-496, 1996.
- 1057 Viers, J., Dupré, B., and Gaillardet, J.: Chemical composition of suspended sediments in  
1058 World Rivers: New insights from a new database, *Science of The Total Environment*, 407(2),  
1059 853-868, 2009.

- 1060 Wallmann, K.: Feedbacks between oceanic redox states and marine productivity: A model  
1061 perspective focused on benthic phosphorus cycling, *Global Biogeochemical Cycles*, 17(3),  
1062 2003.
- 1063 Wallmann, K.: Phosphorus imbalance in the global ocean?, *Global Biogeochemical Cycles*,  
1064 24(4), 2010.

1065 **Tables**

1066 **Table 1:** Station list for the sites of the benthic lander (BIGO), multi-corer (MUC) and CTD deployments including the bottom water  
 1067 concentrations of oxygen (O<sub>2</sub>), nitrate (NO<sub>3</sub><sup>-</sup>) and sulfide (H<sub>2</sub>S) in μM. The station numbers were according to Dale et al., 2015. bdl=below  
 1068 detection limit (5 μM)

Nr.	Station	Gear	Date (2013)	Longitude (°W)	Latitude (°S)	Water depth (m)	BW O <sub>2</sub> (μM)	BW NO <sub>3</sub> <sup>-</sup> (μM)	BW H <sub>2</sub> S (μM)
	98	CTD26	14.01.	12°13.504'	77°10.799'	75			
I	220	MUC39	25.01.	12°13.531'	77°10.061'	72	bdl	-	33.22
	110	BIGO1-2	15.01.	12°13.506'	77°10.793'	74			
	269	CTD79	29.01.	12°16.690'	77°14.999'	128			
III	248	MUC46	27.01.	12°16.697'	77°15.001'	129	bld	0.02	-
	165	BIGO2-4	20.01.	12°16.690'	77°14.995'	128			
	111	CTD29	15.01.	12°18.729'	77°17.757'	145			
IV	36	MUC10	09.01.	12°18.708'	77°17.794'	145	bdl	7.1	
	57	BIGO1-1	11.01.	12°18.711'	77°17.803'	141			
	279	CTD81	30.01.	12°21.490'	77°21.713'	195			
V	247	MUC45	27.01.	12°21.491'	77°21.702'	195	bdl	6.3	-
	201	BIGO1-4	23.01.	12°21.502'	77°21.712'	195			
	92	CTD24	13.01.	12°23.300'	77°24.200'	244			
VI	198	MUC34	23.01.	12°23.300'	77°24.228'	244	bdl	11.9	-
	74	BIGO2-2	12.01.	12°23.300'	77°24.186'	244			

	66	CTD16	12.01.	12°27.535'	77°29.593	414			
VIII	107	MUC23	15.01.	12°27.198'	77°29.497'	407	bdl	12.1	-
	207	BIGO2-5	24.01.	12°27.207'	77°29.517'	409			

---

1069



1070 **Table 2:** Equations for the P mass balance calculations. Results are shown in Table 4.

---

**Equations for P mass balance calculations**

---

**P Input to the sediments ( $\text{mmol m}^{-2} \text{d}^{-1}$ )**

- (4) Total particulate phosphorus rain rate  $RR_{TPP} = RR_{PIP} + RR_{POP} = F_{TPPO4} + F_{Pbur}$
- (5) Particulate inorganic phosphorus rain rate  $RR_{PIP} = RR_{POC} / \left(\frac{POC}{PIP}\right)$
- (6) Particulate organic phosphorus rain rate  $RR_{POP} = RR_{POC} / \left(\frac{POC}{POP}\right)$
- (7) Terrigenous P input ( $P/Al = 0.02$ , Vier et al., 2009)  $RR_{Pterr} = Al_{(0-1)} * MAR * \frac{P}{Al}$

**P Burial in the sediments ( $\text{mmol m}^{-2} \text{d}^{-1}$  and  $\text{g m}^{-2} \text{d}^{-1}$ ) at 11 cm**

- (8) Phosphorus burial flux  $F_{Pbur} = MAR * P_{11}$
- (9) Mass accumulation rate  $MAR = \rho_{dry} * (1 - \phi_{\infty}) * SR$
- (10) TPP burial efficiency  $PBE = MAR * \left(\frac{P_{11}}{RR_{TPP}}\right) * 100 \%$

**P release from the sediments ( $\text{mmol m}^{-2} \text{d}^{-1}$ )**

Benthic P fluxes ( $F_{TPPO4}$ ) and the potential diffusive P fluxes were determined as described in the methods

- (11) P release from POP degradation according to Redfield ( $C/P = 106$ )  $F_{P(Red)} = F_{DIC}/106$
- (12) True P release from POP  $F_{P(POP)} = F_{DIC} / \left(\frac{POC}{POP}\right)$
- (13) P release from total particulate phosphorus  $F_{P(TPP)} = F_{DIC} / \left(\frac{POC}{TPP}\right)$
- (14) P release from the dissolution of Fe (oxyhydr)oxides ( $Fe/P = 10$ , Slomp et al., 1996)  $F_{P(Fe)} = F_{Fe2+} / \left(\frac{Fe}{P}\right)$
- (15) P deficit to outbalance the P budget  $F_{P(deficit)} = RR_{TPP} + RR_{terr} + F_{P(Fe)} - (F_{TPPO4} + F_{Pbur})$
- 

1071

1072

1073 **Table 3:** In situ benthic chamber TPO<sub>4</sub> fluxes in mmol m<sup>-2</sup> d<sup>-1</sup> along the 12°S transect. The  
 1074 numbers are shown as an average calculated from the minimum and maximum flux  
 1075 determined from two benthic chambers.

Station		Water depth (m)	F <sub>TPO4</sub> (mmol m <sup>-2</sup> d <sup>-1</sup> )
I	BIGO1_2	74	1.04 ± 0.31
II	BIGO1_5	101	0.35 ± 0.01
III	BIGO2_4	128	0.30 ± 0.05
IV	BIGO1_1	141	0.23 <sup>a</sup>
V	BIGO1_4	195	0.12 <sup>a</sup>
VI	BIGO2_2	243	0.44 ± 0.07
VII	BIGO2_1	306	0.26 ± 0.04
VIII	BIGO2_5	409	-0.07 <sup>a</sup>
IX	BIGO2_3	756	0.06 <sup>a</sup>
X	BIGO1_3	989	0.02 ± 0.02

1076 <sup>a</sup> only one benthic flux was measured

1077 **Table 4:** Measured and calculated parameters for the P mass balance along the 12°S transect. The numbers in front of key parameters  
 1078 correspond to equations in Table 2.

12°S	Transect section I		Transect section II			Phosphorite formation
	Station I 74 m	Station III 128 m	Station IV 141 m	Station V 195 m	Station VI 244 m	Station VIII 407 m
<b>Benthic chamber TPO<sub>4</sub> flux (F<sub>TPO4</sub>)*</b> mmol m <sup>-2</sup> d <sup>-1</sup>	1.04 ± 0.31	0.3 ± 0.05	0.23 -	0.12 -	0.44 ± 0.07	-0.07 -
<b>Potential (diffusive) TPO<sub>4</sub> flux (pot. F<sub>TPO4</sub>)</b> mmol m <sup>-2</sup> d <sup>-1</sup>	1.07 ± 0.23	2.0 -	0.5 -	1.6	1.5 -	
<b>Relative abundance of Marithioplococci-related bacteria*</b> copies g <sup>-1</sup> (0-5 cm sediment depth)	4159		1687	3072		190
<b>Benthic chamber DIC flux (F<sub>DIC</sub>)**</b> mmol m <sup>-2</sup> d <sup>-1</sup>	65.9 ± 21	20.4 ± 7	8 ± 0.4	3.2 ± 1	4.7 ± 1	2.2 ± 0.3
<b>POC rain rate (RR<sub>POC</sub>)**</b> mmol m <sup>-2</sup> d <sup>-1</sup>	79.5 ± 33	28.2 ± 12	10.5 ± 3	12.5 ± 6	10.6 ± 4	2.7 ± 1
<b>Sediment accumulation rate (ω<sub>acc</sub>)**</b> cm yr <sup>-1</sup>	0.45 ± 0.09	0.2 ± 0.04	0.04 ± 0.008	0.1 ± 0.02	0.07 ± 0.014	0.01 ± 0.002
<b>Mass accumulation rate (MAR)**</b> g m <sup>-2</sup> yr <sup>-1</sup>	1800 ± 360	600 ± 120	128 ± 26	320 ± 64	182 ± 37	44 ± 9
Ratios for particulate matter from the water column (2 to 5 m above the sea floor):						
<b>POC/PPP*</b>	76 ± 4	68 ± 9	94 ± 10	132 ± 36	62 ± 9	96 ± 9
<b>POC/PIP*</b>	197 ± 17	125 ± 34	291 ± 79	385 ± 7	217 ± 34	209 ± 34
<b>POC/POP*</b>	126 ± 17	149 ± 29	142 ± 3	214 ± 87	87 ± 29	178 ± 29
<b>(4) TPP rain rate (RR<sub>TPP</sub>)</b>	1.00 ± 0.31	0.40 ± 0.09	0.11 ± 0.02	0.09 ± 0.02	0.17 ± 0.02	0.03 ± 0.01

mmol m <sup>-2</sup> d <sup>-1</sup>							
<b>(5) PIP rain rate (RR<sub>PIP</sub>)</b>	0.39 ± 0.14	0.22 ± 0.04	0.04 ± 0	0.03 ± 0.02	0.05 ± 0.01	0.01 ± 0.01	
mmol m <sup>-2</sup> d <sup>-1</sup>							
<b>(6) POP rain rate (RR<sub>POP</sub>)</b>	0.61 ± 0.18	0.18 ± 0.05	0.07 ± 0.02	0.06 ± 0.01	0.12 ± 0.01	0.01 ± 0.01	
mmol m <sup>-2</sup> d <sup>-1</sup>							
<b>(7) Terrigenous P input (RR<sub>Pterr</sub>)</b>	0.10 -	0.02 -	0.01 -	0.02 -	0.01 -	0.00 -	
<b>(8) Burial flux (F<sub>Pbur</sub>) in 11 cm sediment depth</b>	0.23 -	0.09 -	0.02 -	0.08 -	0.04 -	0.13 -	
mmol m <sup>-2</sup> d <sup>-1</sup>							
<b>Avg. Al conc. (0-1 cm sediment)</b>							
<b>(Al<sub>0-1</sub>)*</b>	0.99 -	0.70 -	1.10 -	0.97 -	0.72 -	0.66 -	
mmol g <sup>-1</sup>							
<b>Avg. P conc. (0- 11 cm sediment)</b>							
<b>(P<sub>11</sub>)*</b>	0.05 -	0.05 -	0.07 -	0.09 -	0.08 -	1.05 -	
mmol g <sup>-1</sup>							
<b>(10) P burial efficiency (PBE) at 11cm sediment depth</b>	26 ± 8	23 ± 4	23 ± 5	92 ± 20	23 ± 2	490 ± 100	
%							
<b>(11) P release from POP degradation according to Redfield (F<sub>P(Red)</sub>)</b>	0.62 ± 0.2	0.19 ± 0.06	0.08 ± 0.01	0.03 ± 0.01	0.04 ± 0.02	0.02 ± 0	
mmol m <sup>-2</sup> d <sup>-1</sup>							
<b>(12) P release from POP degradation (F<sub>P(POP)</sub>)</b>	0.52 ± 0.16	0.14 ± 0.05	0.06 ± 0.01	0.02 ± 0.01	0.05 ± 0.02	0.01 ± 0	
mmol m <sup>-2</sup> d <sup>-1</sup>							
<b>(13) P release from TPP degradation (F<sub>P(TPP)</sub>)</b>	0.87 ± 0.17	0.3 ± 0.1	0.09 ± 0.01	0.02 ± 0.01	0.08 ± 0.02	0.02 ± 0.01	
mmol m <sup>-2</sup> d <sup>-1</sup>							
<b>Benthic diffusive TPO<sub>4</sub> flux (potential P flux)*</b>	1.08 ± 0.23	2.0 -	0.5 -	1.6 -	1.5 -	- -	
<b>Diffusive Fe<sup>2+</sup> flux (F<sub>Fe2+</sub>)*</b>	0.04 ± 0.02	0.01 -	0.02 -	0.0 -	0.03	0.0	

**(14) P release from**

**Fe (oxyhydr)oxides ( $F_{P(Fe)}$ )**  
mmol m<sup>-2</sup> d<sup>-1</sup>

0.004 ± 0.002 0.001

0.002

0.0

0.003

0.0

**(15) P required to outbalance the P**

**budget ( $F_{P(deficit)}$ )**  
mmol m<sup>-2</sup> d<sup>-1</sup>

- -

0.12 -

0.09 -

0.3 -

-

1079 \* this study

1080 \*\*published data from Dale et al. (2015)

1081 **Figure captions**

1082 **Figure 1:** Study area, sampling stations and O<sub>2</sub> concentration in μM along the 12°S transect.

1083 **Figure 2A:** Concentration profiles of TPP, PIP, POP and POC of the water column particles  
1084 and the surface sediments along the 12°S transect. Water column particle concentrations  
1085 (upper panel) are given in μmol L<sup>-1</sup> and surface sediment concentrations (lower panel) are  
1086 shown in μmol mg<sup>-1</sup>. Note that the water column particle concentrations shown for station VI  
1087 (244 m) at 10 m water depth are ~ 5 times higher than at the other stations.

1088 **Figure 2B:** Ratios of POC to TPP, PIP and POP (POC/xP) along the 12°S depth transect of  
1089 water column particles and surface sediments (0 – 5.5 cm depth) of station I to VIII (74 to 407  
1090 m).

1091 **Figure 3:** Average distribution of POP and PIP (%) per station in the water column particles  
1092 and in the top 5.5 cm of the sediments.

1093 **Figure 4A:** Measured benthic TPO<sub>4</sub> fluxes (mmol m<sup>-2</sup> d<sup>-1</sup>) at 12°S. The black line shows the  
1094 theoretical TPO<sub>4</sub> flux generated from organic matter degradation with a Redfield POC/POP  
1095 ratio of 106.

1096 **Figure 4B:** Potential TPO<sub>4</sub> fluxes (mmol m<sup>-2</sup> d<sup>-1</sup>) calculated from porewater profiles  
1097 compared to the measured benthic TPO<sub>4</sub> fluxes (mmol m<sup>-2</sup> d<sup>-1</sup>) at stations I to VIII (74 to 407  
1098 m). The black line with triangles depicts the TPO<sub>4</sub> flux that could be generated during  
1099 degradation of total particulate phosphorus.

1100 **Figure 4C:** P percentages of the different P sources and the missing P that is needed to  
1101 maintain the measured TPO<sub>4</sub> release rates and P burial fluxes for stations IV, V and VI (141,  
1102 195 and 244 m) of transect section II. The missing P is assumed to be supplied by sulfide-  
1103 oxidizing Marithioploca-related bacteria (see Discussion).

1104 **Figure 5:** Mass balance calculations and measured benthic TPO<sub>4</sub> fluxes for stations I to VIII  
1105 (74 to 407 m). All fluxes are in mmol m<sup>-2</sup> d<sup>-1</sup>.

1106 **Figure 5A:** POP rain rates, TPO<sub>4</sub> fluxes and P burial rates only. The number in percent  
1107 denotes missing P needed to sustain the benthic TPO<sub>4</sub> fluxes.

1108 **Figure 5B:** Mass balance calculations including the POP and PIP rain rates, the terrigenous P  
1109 input, P release from the reductive dissolution of Fe (oxyhydr)oxides and the benthic TPO<sub>4</sub>  
1110 fluxes into the bottom waters as well as the P burial rates.

1111 **Figure 6:** Measured benthic TPO<sub>4</sub> fluxes versus relative abundance of *Marithioploca* in cells  
1112 g<sup>-1</sup> in the upper 5 cm of the sediment. Highest abundance and TPO<sub>4</sub> flux was found at station  
1113 I. The other data points are for the stations IV, VI and VIII (with decreasing abundance and  
1114 TPO<sub>4</sub> flux).

1115 **Figure 7:** Comparison of porewater PO<sub>4</sub><sup>3-</sup> concentrations (blue) before and after the  
1116 freeze/thaw experiments (red) in μmol L<sup>-1</sup>.

The following pages contain one figure per page and the supplementary material. The single figures are not labeled, but there are in the following order:

Fig. 1

Fig. 2A

Fig. 2B

Fig. 3

Fig. 4

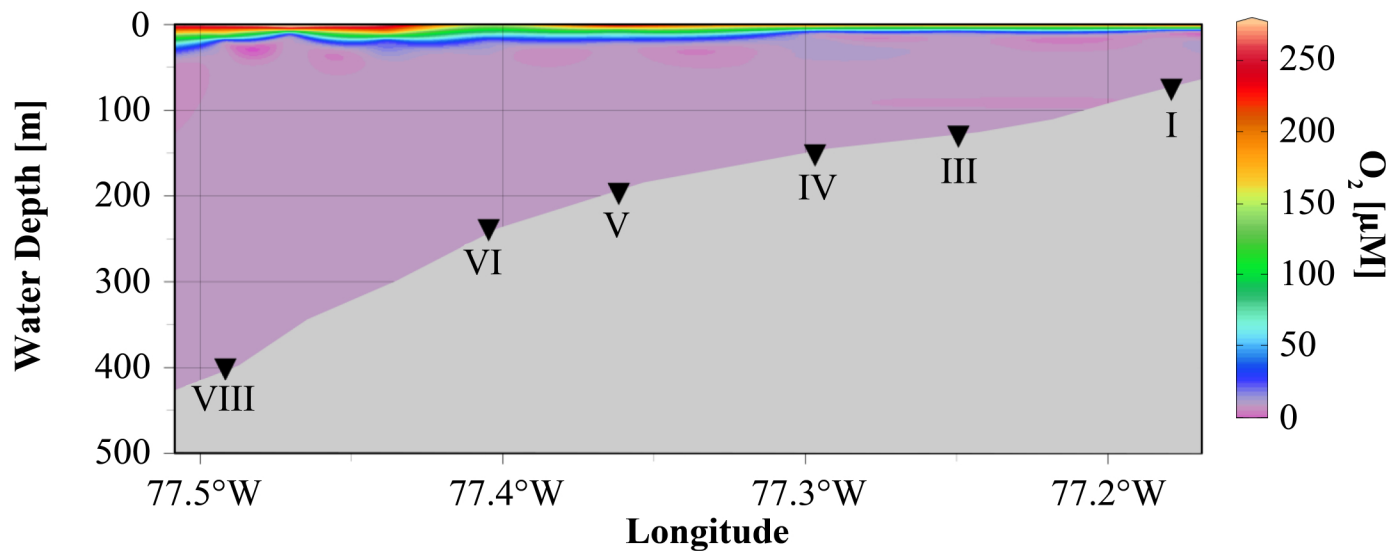
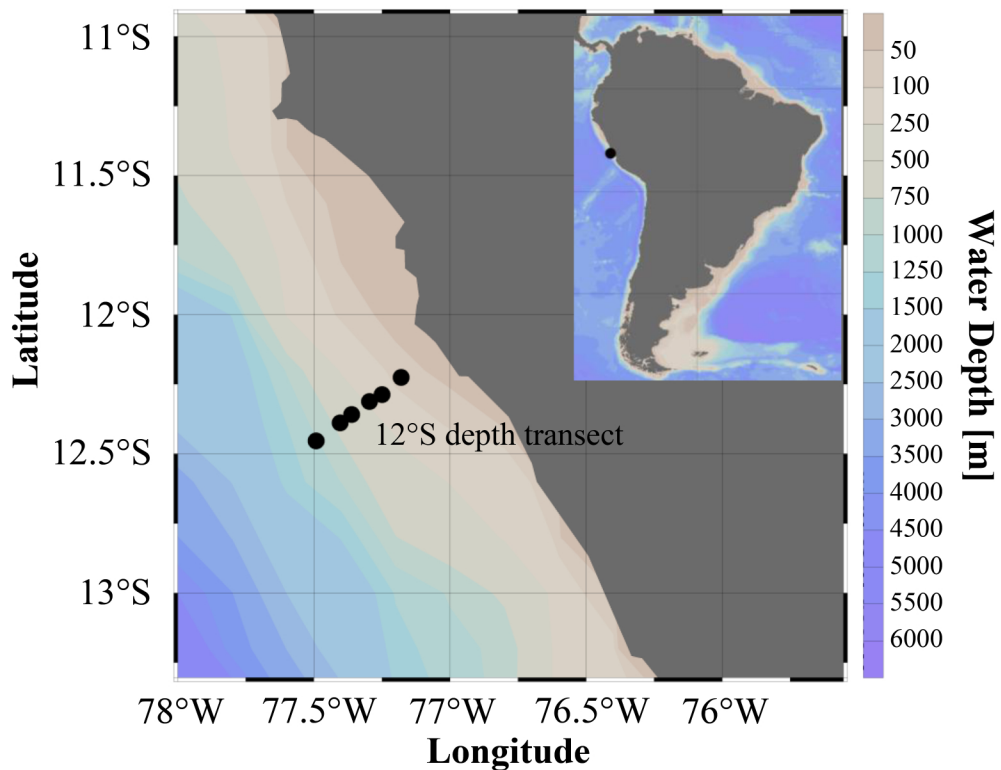
Fig.5

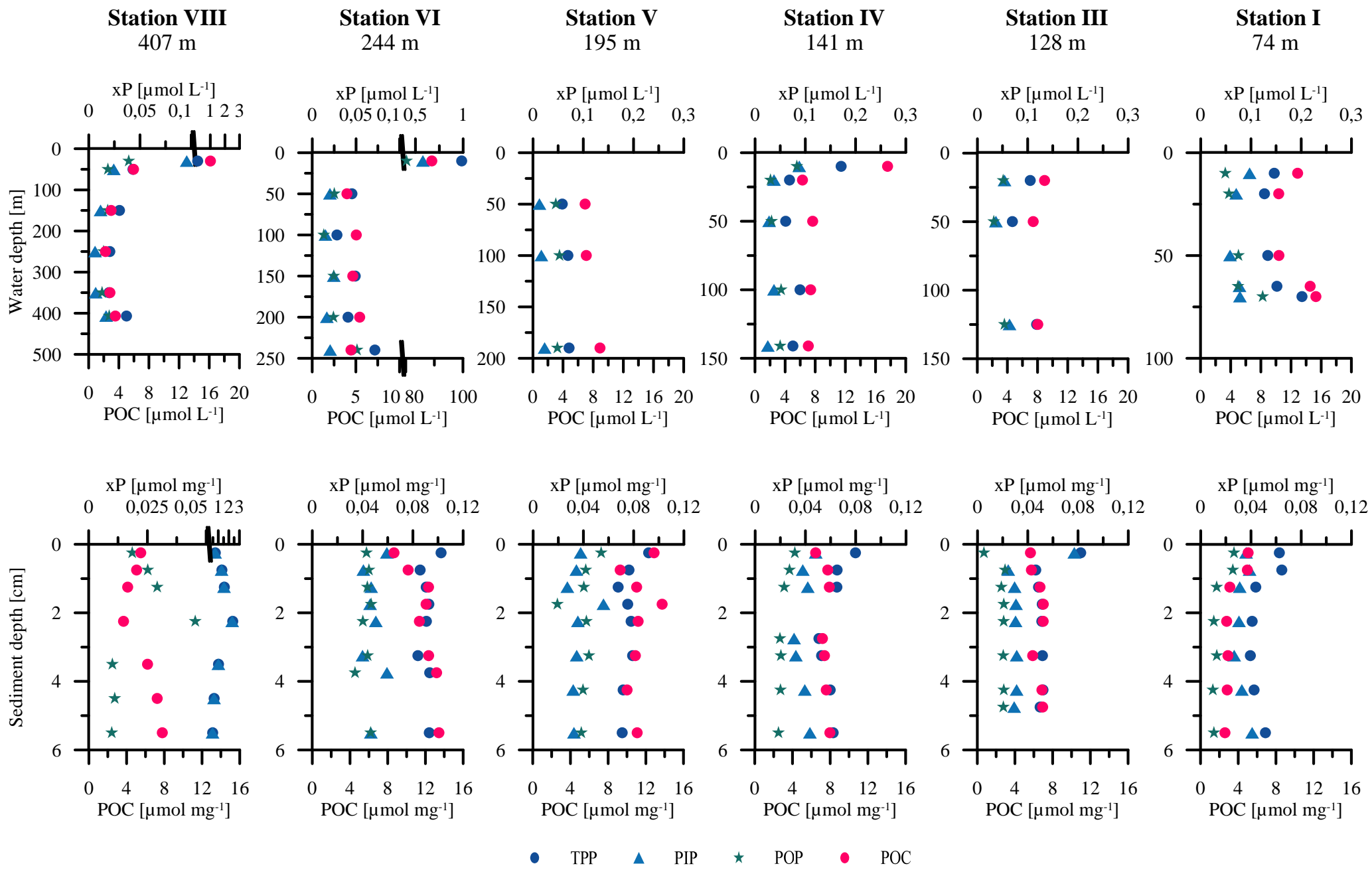
Fig. 6

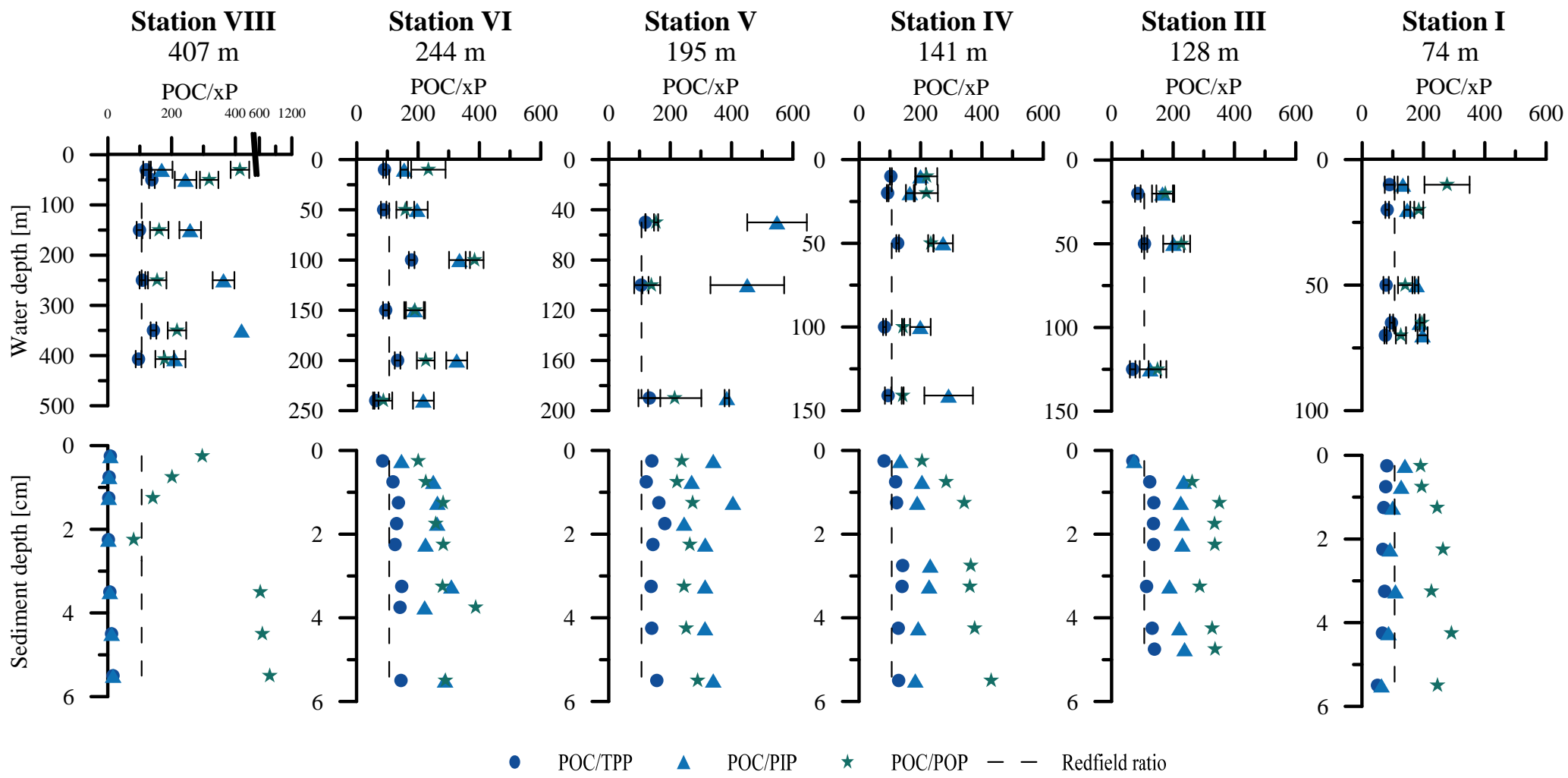
Fig. 7

Supplementary material

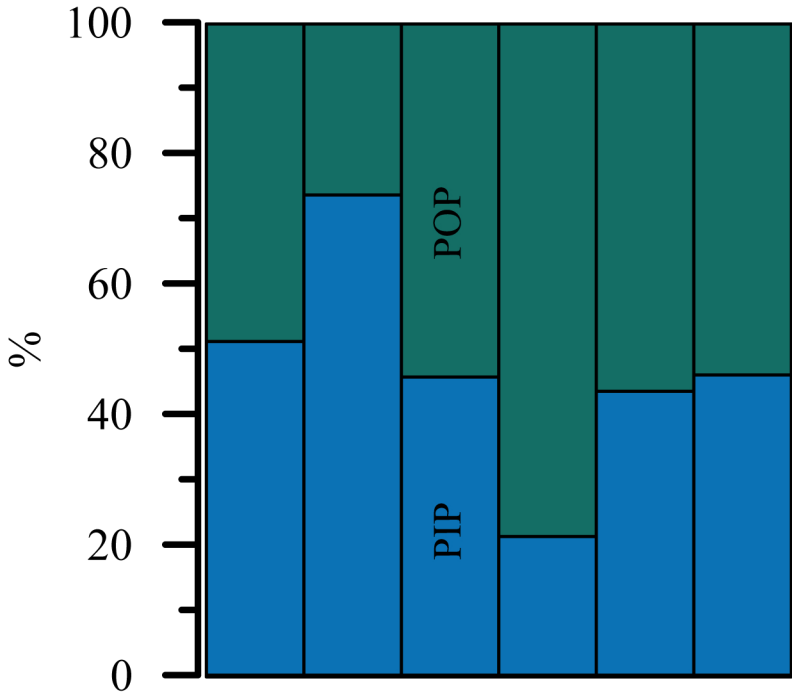




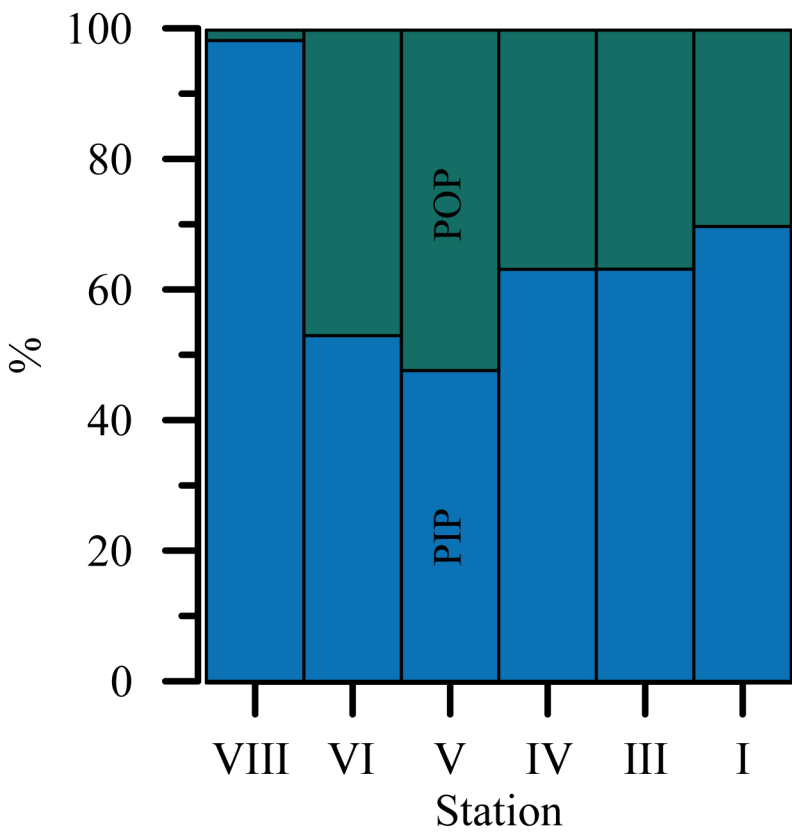


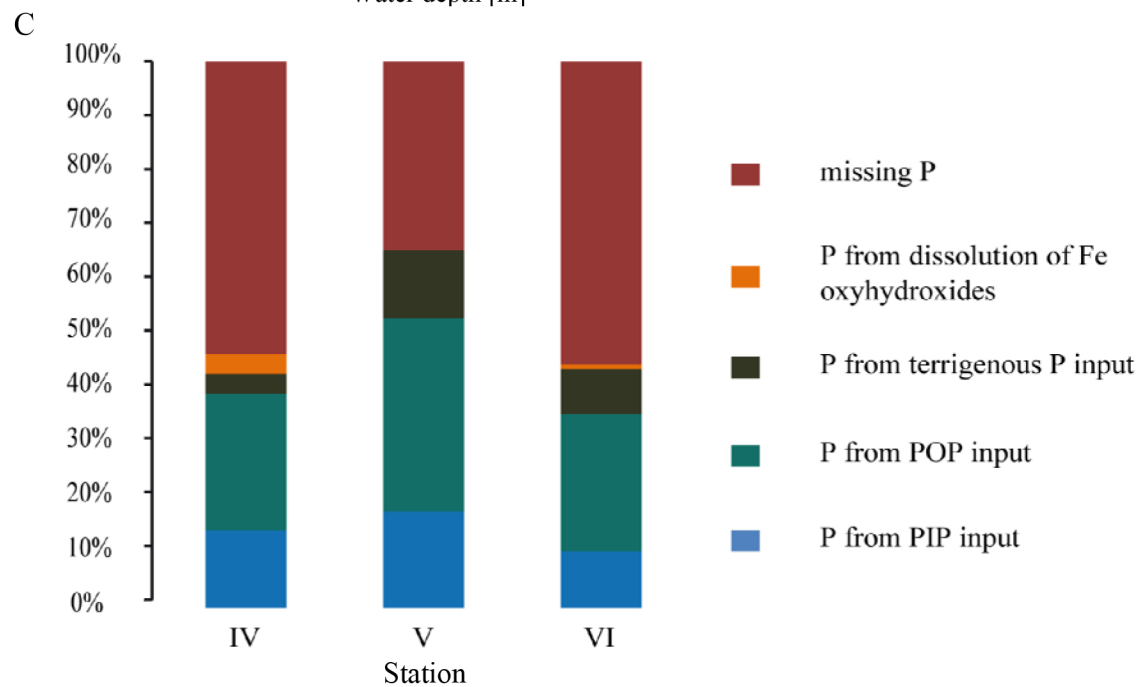
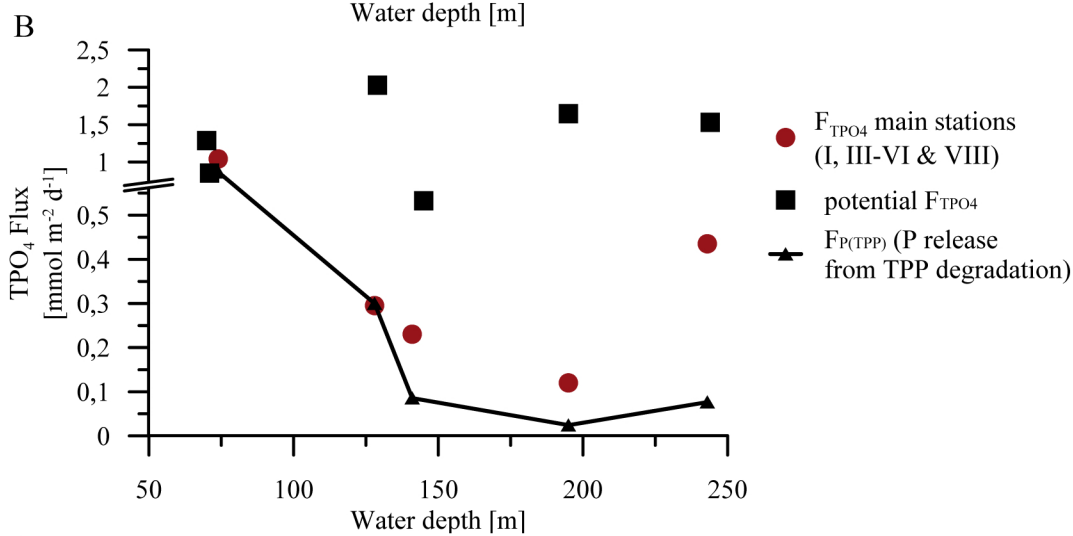
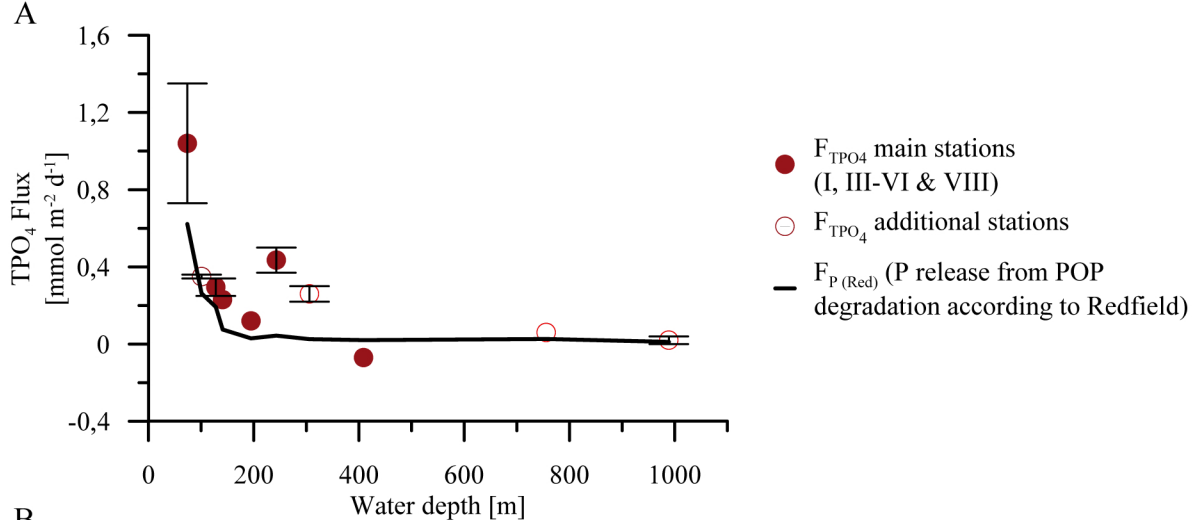


# Water column particles



# Sediments

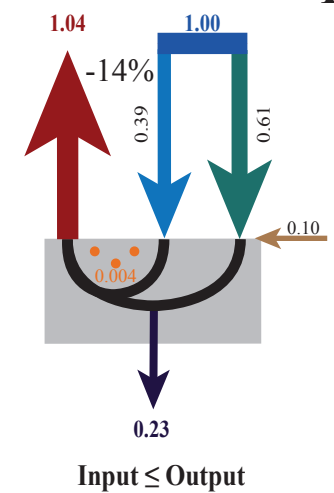
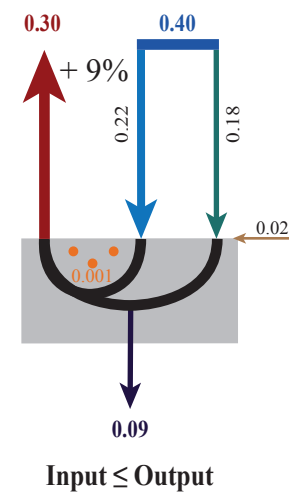
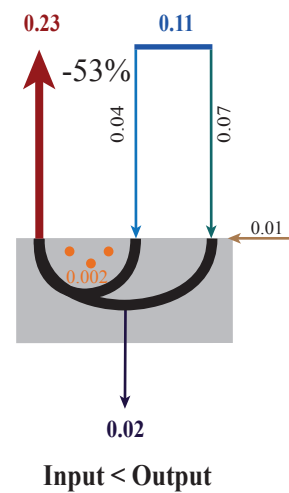
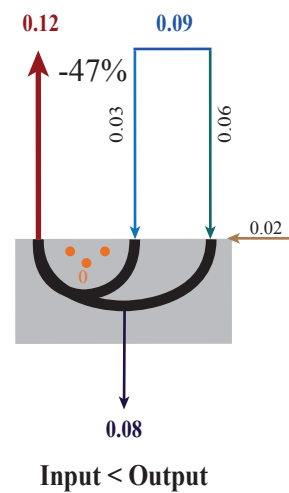
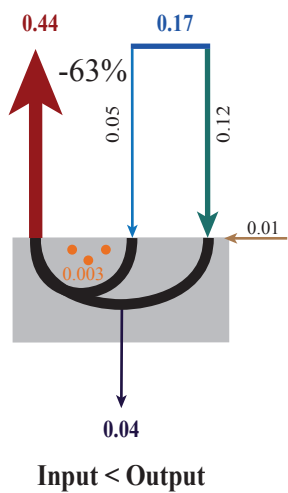
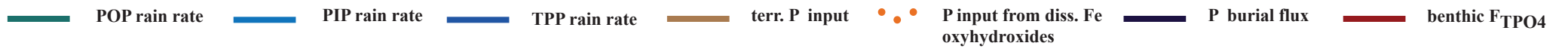
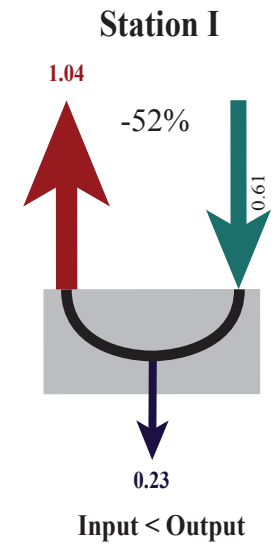
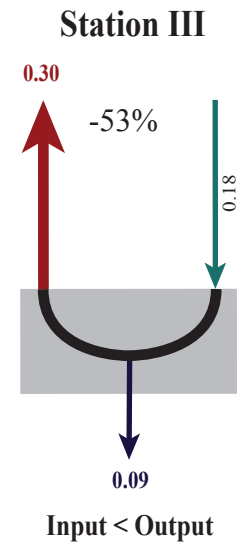
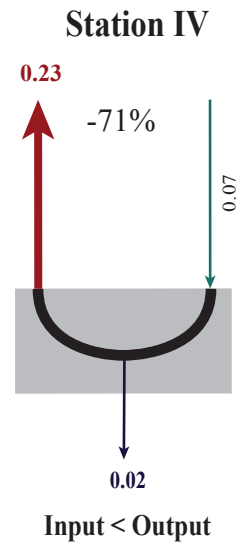
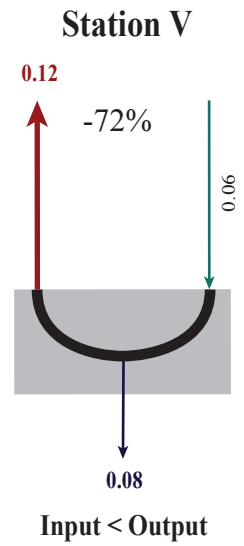
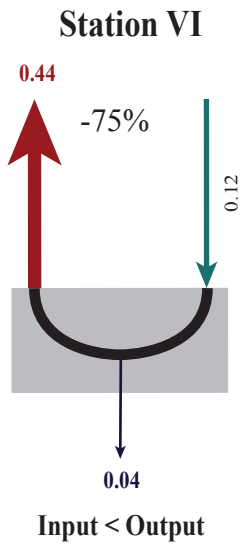




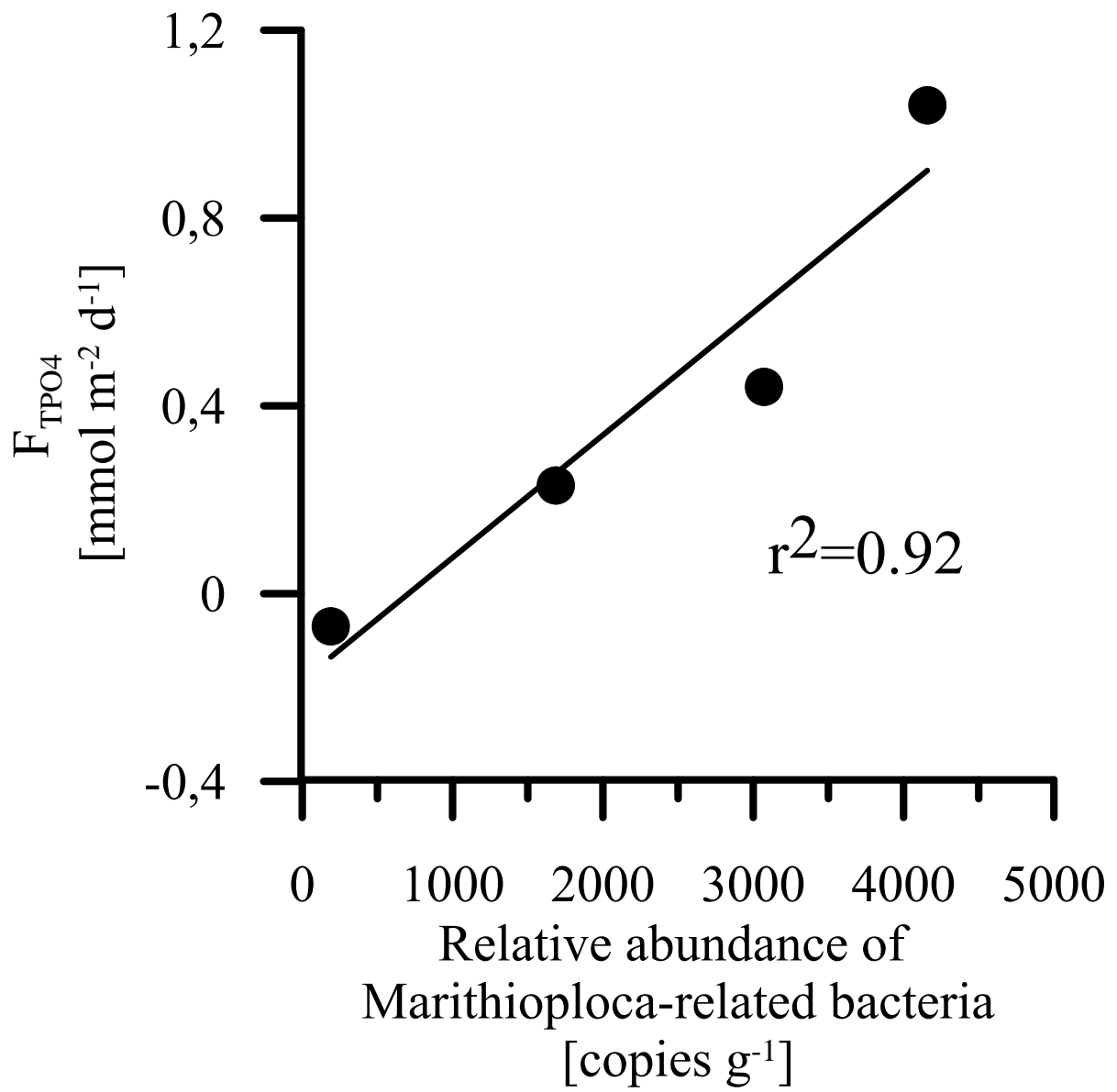
Transect section II

Transect section I

A



B



### Transect section II

### Transect section I

